J Mater Sci (2012) 47:7417–7438
DOI 10.1007/s10853-012-6425-z

FIRST PRINCIPLES COMPUTATIONS

Growth and interfacial properties of epitaxial oxides on semiconductors: ab initio insights

Kevin F. Garrity · Alexie M. Kolpak · Sohrab Ismail-Beigi

Received: 23 January 2012 / Accepted: 17 March 2012 / Published online: 3 May 2012

Abstract Crystalline metal oxides display a large number of physical functionalities such as ferroelectricity, magnetism, superconductivity, and Mott transitions. High quality heterostructures involving metal oxides and workhorse semiconductors such as silicon have the potential to open new directions in electronic device design that harness these degrees of freedom for computation or information storage. This review describes how first-principles theoretical modeling has informed current understanding of the growth mechanisms and resulting interfacial structures of crystalline, coherent, and epitaxial metal oxide thin films on semiconductors. Two overarching themes in this general area are addressed. First, the initial steps of oxide growth involve careful preparation of the semiconductor surface to guard against amorphous oxide formation and to create an ordered template for epitaxy. The methods by which this is achieved are reviewed, and possibilities for improving present processes to enable the epitaxial growth of a wider set of oxides are discussed. Second, once a heterointerface is created, the precise interfacial chemical composition and atomic structure is difficult to determine unambiguously from experiment or theory alone. The current understanding of the structure and properties of complex oxide/semiconductor heterostructures is reviewed, and the main challenges to prediction—namely, (i) are these heterostructures in thermodynamic equilibrium or kinetically trapped, and (ii) how do the interfaces modify or couple to the degrees of freedom in the oxide?—are explored in detail for two metal oxide thin films on silicon. Finally, an outlook of where theoretical efforts in this field may be headed in the near future is provided.

K. F. Garrity
Department of Physics and Astronomy, Rutgers University, Piscataway, NJ 08854-8019, USA

A. M. Kolpak
Department of Materials Science and Engineering, Massachusetts Institute of Technology, Cambridge, MA 02139, USA

S. Ismail-Beigi (✉)
Department of Applied Physics, Yale University, New Haven, CT 06520, USA
e-mail: sohrab.ismail-beigi@yale.edu

Introduction

With little exaggeration, one can state that the controllable growth of thin films of insulating oxides on semiconductors underpins the digital information age. Being able to reproducibly create or deposit very high quality insulating oxides on silicon with very low densities of interfacial defects has allowed the simple metal-oxide-semiconductor field effect transistor (MOSFET) to be produced in astronomical numbers and at very small cost: it is estimated that more than 10^{18} transistors were produced in 2010 [1]. Until recently, the most important oxide has been the native amorphous oxide of silicon, SiO_2, which forms readily and produces a nearly perfect interface on the (001) face of silicon. More recently, transition metal oxides have become more prevalent insulators due to their higher dielectric constants ("high-k") which allow for thicker oxide films and less leakage but otherwise preserve the device characteristics [2]. Enormous research efforts have gone into (and continue to go into) developing and advancing Si-based MOSFETs, and this level of work has allowed the speed and density of transistors to increase exponentially for decades, doubling roughly every 18 months—an observation known as Moore's law [3, 4].

Past and present generations of transistors use amorphous oxides as insulators. There are many experimental and practical advantages to the amorphous state: isotropy of properties; relative ease of creation or deposition; uniformity; and lack of problem with polycrystalline granularity and concomitant grain boundaries. However, the use of amorphous oxides has greatly limited the application of modern electronic structure techniques to practical oxide interface systems due to the complex and aperiodic nature of the amorphous state. From a computational perspective, the necessity for large simulation cells to capture a physically relevant realization of the amorphous state makes performing computations with reliable first-principles electronic structure methods very challenging, if not impossible. To perform such calculations, one must limit the simulated cell size, which can lead to the unphysical dependence of many predicted properties on the specific realization of the disordered state that one employs. In addition, restrictions on the cell size may also exaggerate the influence of boundary conditions at the edge of the simulation cell.

From a purely theoretical angle, one obvious way to circumvent these difficulties is to study a fully crystalline oxide on a semiconductor with a coherent epitaxial interface. The periodicity of the crystalline state then allows one to use periodic boundary conditions and modestly-sized simulation cells (in the interfacial plane). Of course, theoretical considerations aside, one might ask whether such systems are experimentally realizable or of any importance for furthering fundamental knowledge and/or developing novel devices. In fact, it turns out that there are a number of compelling reasons for studying such systems.

Since 1998 [5], growth procedures have been devised that permit various binary alkaline earth oxides, as well as a limited number of complex (perovskite) oxides, to be grown epitaxially on well-known semiconductors such as Si or Ge. For a review of the experimental status, see [6]. Figure 1 shows a high resolution image of the epitaxial interface that is formed when the crystalline perovskite oxide $SrTiO_3$ is grown on Si (001). The presence of an ordered and periodic interface means that a number of advanced characterization techniques that are not applicable to or as useful for amorphous systems can be used to study the crystalline systems during or after growth, e.g., diffraction-based methods using X-rays or electrons as well as high resolution transmission electron microscopy (TEM) methods.

However, beyond the fact that one can grow and characterize crystalline oxides on semiconductors, the possibility of integrating complex transition metal oxides with semiconductor platforms is of great interest because it allows for the harnessing of the functional properties of the transition metal oxide film. Crystalline transition metal oxides display a variety of interesting and potentially useful physical phenomena besides merely being high-k: these phenomena include ferroelectricity, magnetism, superconductivity, Mott physics, and metal–insulator transitions [8]. Coupling these degrees of freedom to the well-developed Si technological platform would allow for the creation of novel types of electronic devices. The simplest example is the ferroelectric field effect transistor (FEFET) [9–12] proposed in the 1950s that involves a ferroelectric in contact with the semiconductor to create a transistor that remembers its state with no power consumption. This feature, enabled by the non-volatile but switchable ferroelectric polarization, would also provide an obvious boon to both memory applications and programmable hardware.

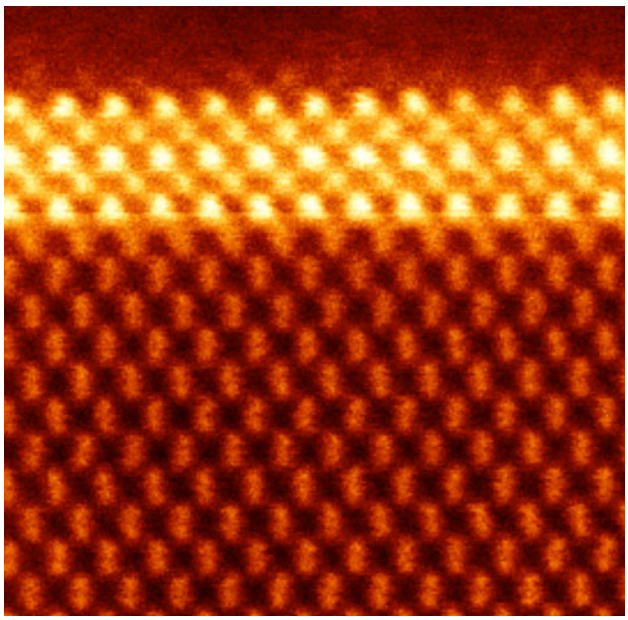

Fig. 1 Scanning transmission electron micrograph (STEM) of an epitaxial 2-unit cell thick film of $SrTiO_3$ grown in the (001) direction on the Si (001) surface. The Si is in the lower portion of the figure while the $SrTiO_3$ occupies the *upper portion* (the *brightest circles* are Sr atoms). The oxide film is clearly strained to the Si substrate and has an abrupt and sharp interface with the semiconductor. The methodologies for growth, characterization, and imaging follow precisely those of Ref. [7]

Regardless of the precise materials choices, first-principles approaches are a critical component of the tools required to understand these systems: ionic and covalent materials are juxtaposed across a sharp interface, and the chemical and electronic behavior of such an environment is generally unknown and difficult to predict reliably from the bulk properties of the constituents or from parametrized models. Hence, first-principles methods are poised to make a number of contributions in this field. Broadly, we see them as twofold.

First, the present experimental growth procedures are somewhat involved as they must avoid the formation of an amorphous layer at the interface (typically SiO_2 or metal-silicides), and the precise reasons for their success or failure are not always understood. This in turn has limited the number of crystalline oxides that can be grown directly on semiconductors. Therefore, one possible contribution from theory is to elucidate what happens during the growth process and how it may be optimized. Section 2 is concerned with these questions.

Second, once the epitaxial thin film is grown, one wishes to understand the chemical composition and atomic geometry of the interfacial region, the electronic properties of the interface (and the thin oxide film), if and how the interfacial region is different from the bulk form of either material, and if and how the interface itself modifies the properties of the thin film (beyond the simple confinement effect of the interface). We describe and address these questions by examining two epitaxial metal oxides on silicon in Sect. 3.

As will be apparent in this review, despite the fact that the presence of an epitaxial interface vastly simplifies the theorists' job in terms of computational modeling, these systems still have a sufficient degree of complexity and a large enough structural phase space that a purely theoretical effort is unlikely to be fruitful. The chemical composition of the interface is in general hard to know a priori, the thermodynamic stability of the various possible interfaces depends strongly on the growth conditions (i.e., chemical potentials of the constituents in the language of thermodynamics) which are very much dependent on the growth recipe and choice of deposition conditions, and in many cases the structure itself is kinetically trapped during and/or after the growth. Therefore, experimental information is necessary to inform the theoretical picture and careful collaboration with experimental colleagues is crucial for building a picture of the physical system. While this does enforce a more modest, nose-to-the-ground mentality on the theorists, in the authors' opinion this is usually a more healthy and generally more productive situation, both in terms of the development of a thorough scientific understanding of the system as well as of discovering potential applications.

Submonolayer alkaline earth oxide template layers

The growth of epitaxial complex oxides on Si requires careful control and preparation of the initial semiconductor surface. In order to achieve an ordered, atomically sharp interface between Si and the desired oxide, the surface must be prepared in a way that both provides an ordered template for oxide growth as well as prevents the formation of undesired and frequently amorphous silicates such as SiO_2 [5, 6, 13–17]. The most successful method for layer-by-layer growth of complex oxides on Si uses molecular beam epitaxy (MBE) and proceeds by first depositing 0.5 monolayer (ML) of an alkaline earth metal, most commonly Sr (Ca and Ba work as well), which both creates an ordered template layer and passivates the surface against SiO_2 formation [5, 6, 13].

Pioneering experimental studies on the growth of epitaxial oxides on Si observed a series of reconstructions during the deposition of the sub-monolayer of Sr on Si. However, the atomic structure corresponding to these reconstructions, their role in passivating the surface, and their temperature dependencies were not well understood [5, 13]. Initial theoretical work investigated the binding of Sr adatoms to a clean and perfectly dimerized Si (001) surface [16]. These calculations identified an especially stable reconstruction at 0.5 ML Sr coverage which corresponds very well to one of the experimentally observed reconstructions, but they were unable to explain several features observed at high temperatures and at intermediate coverages during the deposition. Unraveling the precise reconstructions seen versus coverage and their temperature dependence was only possible after a careful collaboration between theory and experiment [15]. This knowledge has both improved our understanding of the previously successful recipes for complex oxide growth as well as enabled new low temperature pathways to oxide epitaxy on semiconductors. In addition, this model system has clarified the difficulties with direct application of available growth techniques to new materials and has suggested possible new growth methods.

This section is organized as follows. Section 2.1 provides a brief review of relevant experiments. First-principles theoretical results on the bonding of submonolayers of Sr to stoichiometric Si surfaces are reviewed in Sect. 2.2: these studies describe the origin of all the structures observed during low temperature Sr deposition. In Sect. 2.3, the structural phase space is expanded to permit for Si diffusion and the presence of non-stoichiometric Si surfaces, both necessary ingredients for explaining the high temperature growth processes actually employed in experiments. Section 2.4 describes in more detail the types of the chemical interactions found between Sr and Si. Sections 2.5–2.6 describe the difficulties that appear when these growth recipes are used to deposit La on Si and then to grow $LaAlO_3$ on Si. The understanding generated from the successful growth of $SrTiO_3$ on Si highlights the differences between $LaAlO_3$ and $SrTiO_3$. Section 2.6 suggests the likely mechanisms that have so far impeded the growth of $LaAlO_3$ on Si and proposes a new, speculative growth method that first-principles computations suggest could lead to successful epitaxial growth of $LaAlO_3$ on Si.

Review of key experiments

Experimentally, the first step of epitaxial oxide growth on Si is to deposit 0.5 ML of Sr or another alkaline earth metal on Si, usually at high temperatures (≈600 °C) [5, 6, 13–15, 18]. This initial layer is known to be atomically flat, homogeneous, and chemically stable. After the deposition of this initial layer, the system is cooled to room temperature and a layer of SrO is deposited [6]. At this point, the interfacial system must be kept at low temperatures to prevent the formation of unwanted silicates (e.g., Sr_2SiO_4, $SrSiO_3$, SiO_2) [14, 19, 20]. Finally, additional layers of the desired oxide (e.g., SrO, BaO, $SrTiO_3$) are deposited by MBE, and the system is then annealed at moderate temperatures (<800 °C) to crystallize the oxide film [5, 6, 14, 15, 19, 21–23].

A variety of experimental techniques have been used to characterize the submonolayer Sr-on-Si surface, including reflection high energy electron diffraction (RHEED) [5, 14, 15], low energy electron diffraction (LEED) [18], scanning tunneling microscopy (STM) [24–26], photo-emission spectroscopy (PES) [27], and synchrotron X-ray diffraction (XRD) [28]. For deposition at room temperature and for low Sr coverages up to 0.5 ML, electron diffraction indicates that the underlying Si surface retains the same 2 × 1 symmetry of the bare dimerized Si (001) surface [15]. In addition, STM images are consistent with Sr adatoms being adsorbed on top of the dimerized Si surface [24]. The Sr adatoms tend to form diagonal chains on the surface but with no long range order.

Deposition at higher temperatures (600 °C) results in a significantly different surface evolution. In particular, diffraction experiments find an ordered 2 × 3 reconstruction which appears at 1/6 ML Sr coverage (see Fig. 6) [5, 14, 15, 18]. STM images of this 1/6 ML reconstruction show an ordered 2 × 3 pattern with strong bias dependence (see Fig. 5) [24–26]. Results at even higher temperatures (800 °C) show that this 2 × 3 reconstruction can be reversibly melted and reformed, and its temperature versus coverage phase boundary has been measured [29].

Above 1/6 ML, the surface transitions back to an ordered 2 × 1 reconstruction, which covers the entire surface at 1/2 ML. Usually, diffraction studies cannot distinguish the relative orientation between the original 2 × 1 bare Si surface and 1/2 ML 2 × 1 structure due to the presence of twinned 2 × 1 and 1 × 2 domains on the bare silicon surface (the twinning is known to maximize the relaxation of surface stress [30]). However, it is well known that a monodomain silicon surface with no twinning can be achieved by using miscut silicon wafers [30]. The miscut angle is known to increase the density of step edges, which favors the formation of double height steps over single height steps and results in a monodomain 2 × 1 surface. Using a miscut Si wafer, it is possible to explicitly show that the relative orientation of the 1/2 ML structure depends on the deposition temperature [15]: for room temperature deposition, the final 2 × 1 surface has the same orientation as the original Si (001) 2 × 1 dimerized surface; however, for high temperature deposition, the final structure is actually 1 × 2, rotated 90° relative to the original dimers.

Sr on stoichiometric Si (001)

Initial density functional theory (DFT) work on the Sr-on-Si system focused on the binding of submonolayers of Sr to the stoichiometric Si surface—by this we mean the ideal Si (001) surface which forms dimers typically in a 2 × 1 pattern around room temperature [16]. This work is relevant to the low temperature deposition of Sr on Si (see the lower path of Fig. 6) when the Si motion is kinetically hindered. Similar to DFT results for Ba on Si [31], one finds for Sr on Si two stable binding sites, with the lower energy site being in the trough between dimer rows, with the Sr equally spaced between four Si dimers (see Fig. 2 for a side view, Fig. 3 for a schematic top view, and Sec. 2.4 for more details on the Sr–Si bonding). To first approximation, the Sr donates two electrons to one of the neighboring dimers, which fully occupies the dangling bonds on that dimer [16, 17, 32].

For coverages up to 1/2 ML, Sr atoms fill in the low energy binding sites [16, 17]. The arrangement of these low energy binding sites is driven primarily by electrostatic attraction between the positively charged Sr adatoms and the negatively charged Si dimers, which accept electrons from the Sr. The resulting low energy configurations of the surface Sr consist of diagonal chain-like structures for coverages ranging from 1/6 to 1/4 ML (See Fig. 3) [16, 24]. There is a very small energy difference between straight chains and zig-zag chains (compare Fig. 3a and 3b), which will lead to disordered chains at any reasonable growth temperature. These results for Sr on the perfect dimerized Si (001) surface are completely consistent with room temperature experimental results, but they cannot explain the ordered 2 × 3 structure observed at 1/6 ML for higher temperatures (see Sect. 2.1; Fig. 6) [15, 17].

At 1/2 ML Sr, all of the low energy binding sites are filled, resulting in an ordered 2 × 1 structure with the same unit cell and orientation as the original bare Si surface. This fact is also consistent with low temperature RHEED results, but cannot explain the 90° rotation that leads to the observed 1 × 2 structure at 1/2 ML Sr for high temperatures [15, 16]. The next section focuses primarily on coverages up to 1/2 ML in order to understand the observed differences between low and high temperature growth. The behavior at higher coverages can be summarized briefly at follows: Above 1/2 ML, there are no

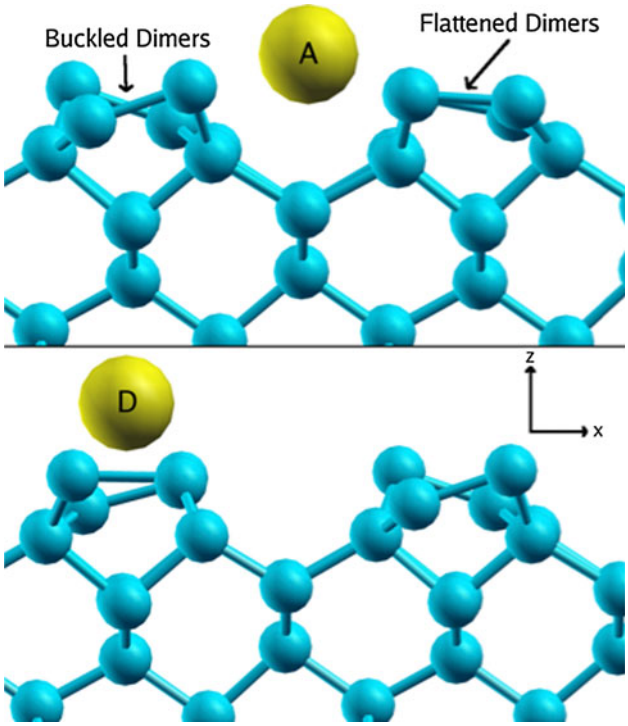

Fig. 2 Side view of lower energy (*top*) and higher energy (*bottom*) binding sites for isolated Sr on Si. Both figures feature both flattened and buckled dimers. The single large (*gold*) sphere in each figure is the Sr adatom, while the Si atoms are the smaller (*blue*) spheres. *Blue* rods connect nearest neighbor Si atoms. Reprinted figure with permission from Ref. [17]. Copyright (2009) by the American Physical Society (Color figure online)

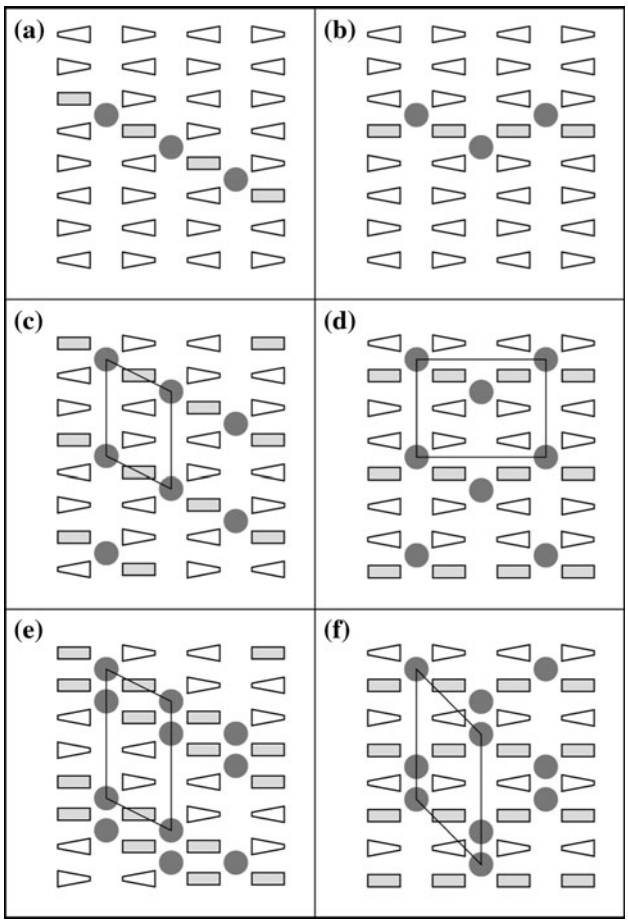

Fig. 3 Schematic *top view* of low coverage Sr on stoichiometric Si structures. All Sr (*gray circles*) are in their low energy binding sites (see Fig. 2, *top*). Buckled Si dimers are represented as *white trapezoids*, with the raised Si as the larger side of the *trapezoid*, and flattened dimers are represented as *gray rectangles*. **a**–**b** Nearly isoenergetic straight and zig-zag chains. **c**–**d** 1/6 ML single chain structures. **e**–**f** Nearly isoenergetic 1/4 ML double chain structures. Reprinted figure with permission from Ref. [16]. Copyright (2004) by the American Physical Society

longer any low energy binding sites available for the additional Sr, and hence the Sr begin to occupy higher energy binding sites on top of the dimer rows [16, 20, 32]. At 2/3 ML coverage, the Si bonding pattern shifts into a 3 × 1 pattern, with 2/3 of the Si dimerized and 1/3 in a nearly ideal 1 × 1 configuration. At 1 ML, the Sr fills every binding site, with some of the Si remaining dimerized in order to increase the distance between Sr adatoms. However, unlike the 1/2 ML structure, which is thermodynamically stable, the thermodynamic ground states for these higher coverages are predicted to involve the reaction of the Si surface and Sr to form silicides (which is expected to happen in experiments at higher growth temperatures which mobilize the Si) [5, 6, 16, 20, 32].

Sr on non-stoichiometric Si surfaces

While the theoretical results of Sect. 2.2 are consistent with low-temperature experiments, they cannot explain the higher temperature RHEED and STM which are more relevant to typical oxide growth conditions (see Sect. 2.1) [6, 15]. In order to understand the system at higher temperatures, it is necessary to enlarge the phase space to include structures with non-stoichiometric Si coverages, by which we mean that a certain fraction of the Si atoms of the originally perfect surface are missing (or equivalently, a sub-monolayer of Si is added to the ideal surface) [17]. Guided by the experimentally observed 2 × 3 reconstruction at 1/6 ML coverage, an investigation of Sr-on-Si surface structures related to low energy defects and steps on the Si (001) surface led to the discovery of a new low energy and thermodynamically stable 2 × 3 structure at 1/6 ML Sr (see Fig. 4) [15, 17]. One set of key experiments that greatly narrowed the phase space for first-principles theory were those performed on the miscut Si wafers [15]: due to the uniform direction of dimers on the surface, electron diffraction during Sr deposition unambiguously revealed that the key structure had 2 × 3 periodicity where the 2-fold direction was parallel to the dimer bonds (and the threefold direction perpendicular).

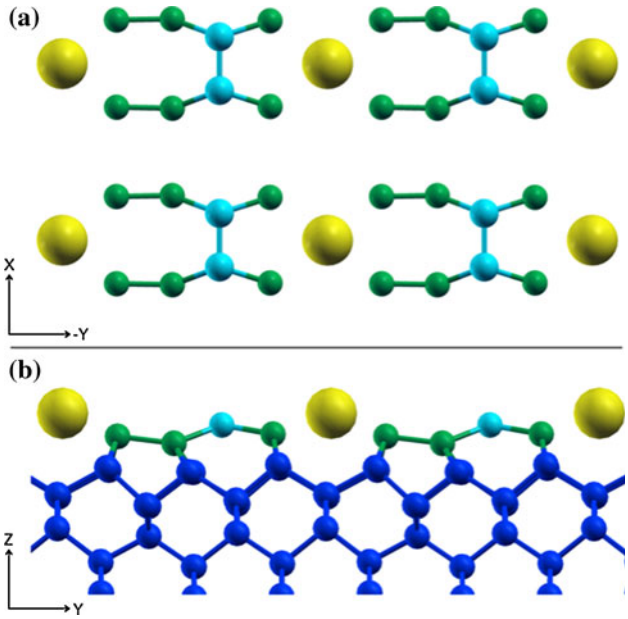

Fig. 4 **a** *Top view* and **b** *side view* of 2 × 3 dimer vacancy structure with 1/6 ML Sr. The Sr atom is large and *yellow*, the silicon dimers from the original surface (1/3 ML silicon) are in *cyan*, the second layer silicon atoms are in *green*, and lower level silicon atoms are in *dark blue*. Reprinted figure with permission from Ref. [17]. Copyright (2009) by the American Physical Society (Color figure online)

The predicted 2 × 3 structure requires removing 2/3 of the original Si dimers from the surface (or equivalently adding 1/3 ML of Si atoms as dimers). The now-exposed second layer Si atoms then reconstruct by forming additional dimer bonds perpendicular to the original dimers, and the Sr occupies the large vacancy which is created by this process. The structure is consistent with existing STM and XRD experiments [17, 25, 26, 28]. Figure 5 shows the experiment/theory comparison for STM.

As explained above, in order to reach this new low energy structure, 2/3 of the surface Si atoms must move across the surface and be removed from the terraces; presumably they must migrate to step edges where they become incorporated into the bulk of the Si (by growing the step edge). This level of Si mobility normally requires high temperatures to overcome the significant energy barriers to Si motion [33]. Energy barriers for isolated Si adatom diffusion on Si (001) are low, but these adatoms tend to meet and form ad-dimers which have large energy barriers of 1.1–1.4 eV, requiring temperatures above 400 °C for significant diffusion [34]. In order to understand the effect of Sr on the kinetic barriers to rearranging Si on the surface, the nudged elastic band (NEB) method [35, 36] was used to calculate the energy barrier for breaking a surface Si dimer bond, as this provides an estimate of the typical barrier to surface Si motion [17]. Adding Sr to the surface is found to continuously and significantly reduce the energy barrier for dimer breaking from 1.3 eV to 0.6 eV as Sr the coverage is increased from 0 to 0.5 ML. In other words, Sr strongly catalyzes the rearrangement of surface Si, lowering the temperature required to form the 1/6 ML structure from what would be expected for a bare Si surface.

This new non-stoichiometric structure is key to understanding the temperature-dependent Sr-on-Si deposition results at both 1/6 ML and 1/2 ML (see Figs. 3, 6) [15, 17]. At low temperatures, Si motion is kinetically limited, the surface Si remains frozen in a 2 × 1 dimerized configuration throughout the Sr deposition, and the Sr fill the low energy binding sites as described in Sect. 2.2. At higher temperatures, the surface is able to overcome the kinetic barriers for Si motion and reach the ground-state structure at 1/6 ML Sr, which requires removal of 2/3 ML Si from the surface. As deposition continues, the additional Sr begins to form regions of the low energy 1/2 ML structure by removing the remaining 1/3 ML of Si (the cyan atoms in Fig. 4). Due to the tetrahedral bonding of the Si, this surface has a full ML of Si removed relative to the original surface and must form a 1 × 2 reconstruction that is perpendicular to the original surface dimers. We emphasize that, physically, the surfaces for 1/2 ML coverage are the same for both low and high temperature deposition, but simply differ by a trivial 90° rotation. This is confirmed indirectly by the fact that epitaxial oxides can be grown with similar quality on either the low temperature 2 × 1 structure or the high temperature 1 × 2 structure. The low temperature path represents a new direction for oxide epitaxy on semiconductors [15].

In addition to the temperature dependence between room temperature and 600 °C, at even higher temperatures (600–800 °C), the 1/6 ML 2 × 3 structure undergoes a reversible melting phase transition [29]. This high temperature disordered phase has been modeled as a lattice gas of Sr adatoms with anisotropic coverage-dependent Sr–Sr interactions where the lattice gas parameters are fit to first-principles DFT calculations [29]. The resulting model is solved at finite temperature by using classical grand canonical Monte Carlo to sample the partition function, which includes the significant configurational entropy of the disordered lattice gas relative to the ordered 2 × 3 structure. The resulting theoretical phase diagram is in quantitative agreement with the experimental one measured by RHEED [29].

Chemistry of Sr on Si (001)

In order to discuss the bonding interactions between Sr and Si, we begin with a brief review of the relevant facts about the Si (001) surface [17, 37]. For an ideally truncated Si (001) surface (i.e., 1 × 1 surface periodicity), each Si atom has two half-filled dangling orbitals. To reduce the number of these orbitals,

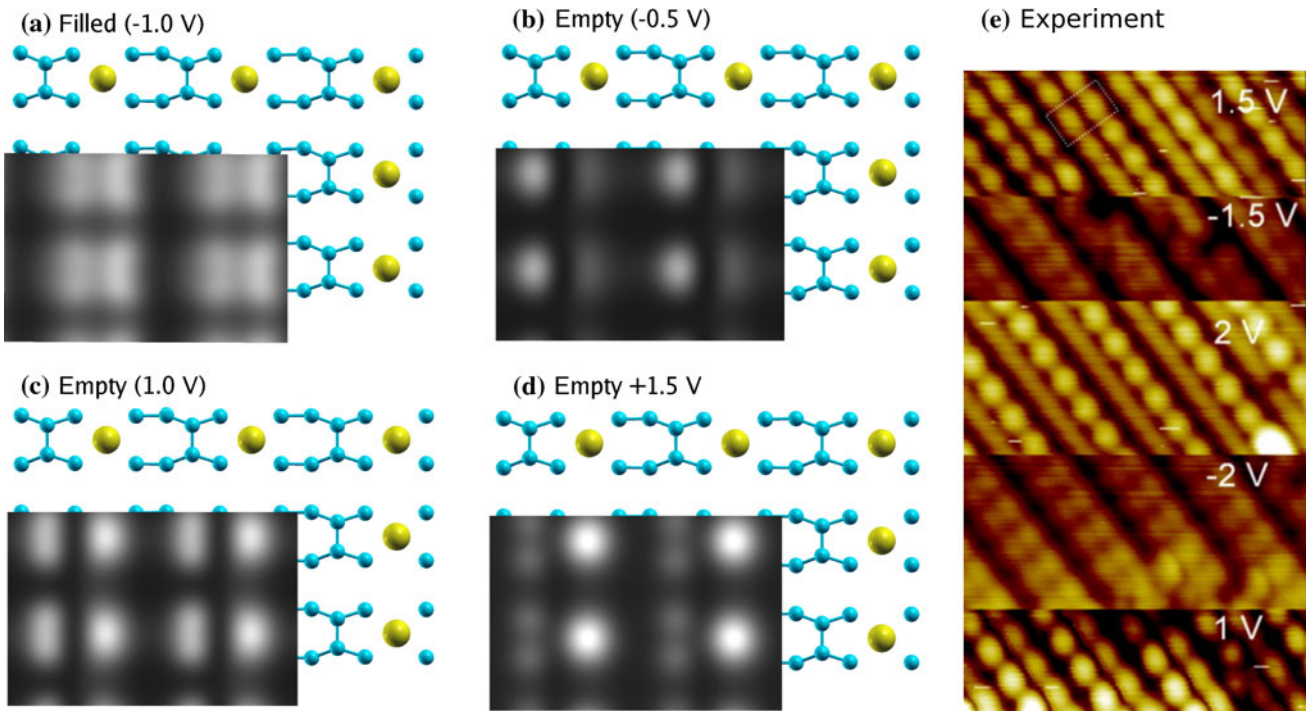

Fig. 5 **a**–**d** Simulated STM [17] of 1/6 ML 2 × 3 Sr-on-Si structure at biases of −1 V, 0.5 V, 1 V, and 1.5 V. **e** Experimental STM [26] at 1.5 V, −1.5 V, 2 V, −2 V, and 1 V (*top to bottom*). The comparison between theory and experiment is best if the empty state theoretical images are compared to experimental ones 0.5 V higher (e.g., compare the 0.5 V theoretical image to the 1.0 V experimental image). This is due to the well-known underestimation of the band gap by in the local density approximation which is numerically close to 0.5 eV for Si. Panels **a**–**d** are reprinted with permission from Ref. [17]. Copyright (2009) by the American Physical Society. Panel **e** is reprinted with permission from Ref. [26]. Copyright (2011) by the American Institute of Physics (Color figure online)

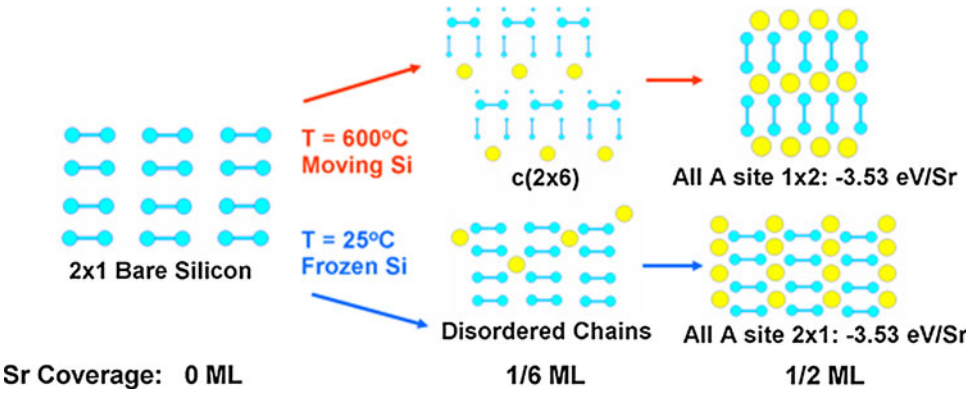

Fig. 6 Schematic temperature-dependent deposition paths for sub-monolayer Sr on Si. Each diagram shows a *top view* of the surface with silicon surface atoms and dimers in *light blue* and the larger Sr in *yellow*. Both the low and high temperature systems begin with a 2 × 1 dimerized bare silicon surface, but as the Sr coverage increases, they follow different paths. At 600 °C, the silicon is quite mobile on the surface, and the surface is at thermodynamic equilibrium at each coverage. However, at 25 °C, silicon motion is prevented by kinetic barriers, the dimers remain intact, and the lowest energy stoichiometric Si surface with Sr adatoms is realized. Reprinted figure with permission from Ref. [17]. Copyright (2009) by the American Physical Society (Color figure online)

the surface breaks symmetry and surface atoms pair up to form additional bonds (dimers) on the surface that are not present in the bulk (see Fig. 2). These dimers line up in rows, resulting in a 2 × 3 reconstruction which greatly stabilizes the surface. In addition, the dimers do not stay flat but buckle: for a flat dimer, each atom still has a single half-filled dangling orbital; when the dimer tilts due to a Jahn–Teller type effect, the raised Si dangling orbital becomes close to sp^3-like and the lowered Si has a dangling orbital that is p_z-like; the lower energy sp^3 state becomes nearly filled while the p_z state becomes nearly empty.

As discussed in Sect. 2.2, to lowest order, the interaction between a Sr adatom and the Si surface is ionic, meaning

that the Sr donates its two valence electrons to the unoccupied dangling (p_z) dimer states. With both dangling orbitals now filled, the driving force for buckling disappears and the dimer flattens again (see Figs. 2, 3). This ionic bonding picture also explains the observed stability of the 2 × 1 0.5 ML structure against oxidation which is the critical role of the Sr layer [27]: at 0.5 ML, there is one Sr for every dimer, so with two donated valence electrons per Sr, all the dimer dangling states are completely filled, and this results in a electronically gapped (semiconducting) surface (See Fig. 7) [16, 17, 32].

While many features of the Sr-on-Si system can be explained via a purely ionic picture, this surface system actually has a significant covalent character in a manner similar to the previously studied Ba on Si system [31]. This covalence is seen by examining electronic densities of states projected on atomic orbitals [16, 32] or Wannier functions [17]. These projected densities of states show significant occupation of Sr *s* and *d* states due to hybridization between Sr and Si (see Fig. 7). The importance of the covalent interactions is exemplified most directly theoretically by comparing the semiconducting 0.5 ML Sr 2 × 1 surface to its higher energy counterpart where all the Sr occupy the higher energy binding site on top of the dimer row. Despite having precisely the same electron count as the low energy 0.5 ML structure, this higher energy structure is in fact metallic [17]. The metallic behavior is due to the decreased overlap between Sr orbitals and the highly direction sp^3-like dangling Si dimer orbitals, and hence the Sr states drop into the Si band gap.

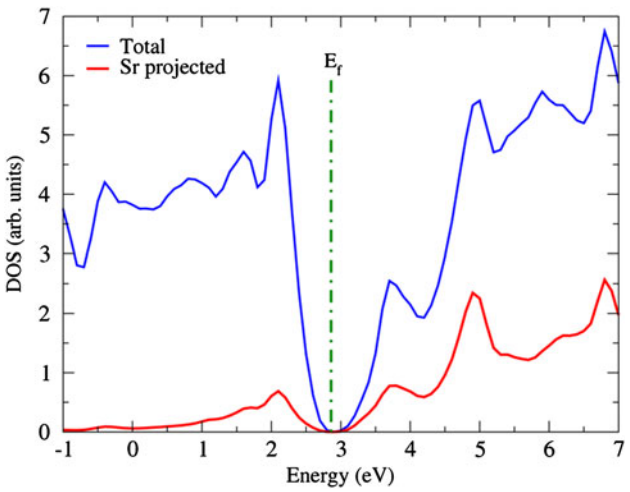

Fig. 7 Total density of states (DOS) in *blue* (*top curve*) and Sr projected DOS onto Sr Wannier functions in *red* (*lower curve*) for the low energy 1/2 ML 2 × 1 structure. The covalent interactions between the Sr states and Si states push the Sr levels above the Fermi level (*vertical dashed*), opening a band gap. Reprinted figure with permission from Ref. [17]. Copyright (2009) by the American Physical Society (Color figure online)

The surprising stability of the 1/6 ML 2 × 3 ground-state structure can be explained by its unusual bonding arrangement (see Fig. 8) [17]. Naively, one would expect this surface system to be metallic: per 2 × 3 area, it has six dangling Si dimer orbitals but only one Sr. However, the surface is in fact semiconducting mainly due to the unusual geometry of the Si dimer from the original surface layer (cyan atoms in Fig. 4a). This dimer is significantly flattened relative to the normal dimers on the bare Si surface, and this flattening causes the atoms forming the dimer to assume a nearly sp^2 character with high energy p_z-like dangling orbitals (see Fig. 8c). These high energy dangling orbitals and the Sr *s* state donate their electrons to the four lower energy sp^3-like danging orbitals that surround the Sr atom (Figs. 8a–b), opening up a gap in the electronic spectrum. This bonding pattern also explains the bias dependence seen in empty state STM images because the dangling p_z-like orbitals and the Sr *s* and *d* states have different energies (see Fig. 5) [25, 26]. Similar STM features are seen for the closely related Sr on Ge system [20].

La on Si

While the Sr-on-Si system provides an effective template layer for epitaxial oxide growth, there is significant interest in expanding the number and types of oxides that one can grow epitaxially and directly on Si [6]. In particular, $LaAlO_3$ appears to be an excellent candidate material because it has the same perovskite structure as $SrTiO_3$ and is closely lattice-matched to Si. In addition, $LaAlO_3$ would be potentially useful as a high-k dielectric material in a silicon field effect transistor since it has a high dielectric constant and favorable band offsets with Si [38–40].

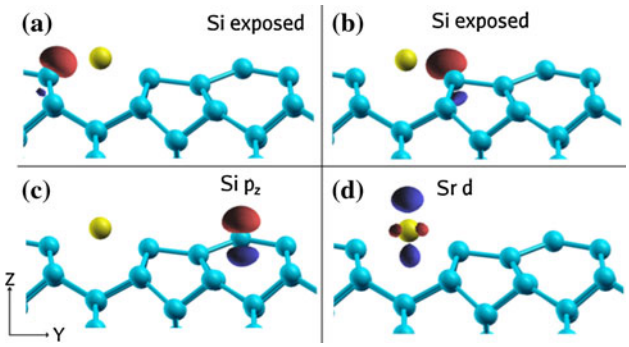

Fig. 8 Side view of the 2 × 3 1/6 ML dimer vacancy structure along with Wannier functions of selected surface states. The larger *yellow ball* is Sr, the smaller *cyan balls* connected by *rods* are Si. *Red* and *blue lobes* show positive and negative isosurfaces of the Wannier functions. **a**, **b** filled dangling orbitals of exposed silicon atoms adjacent to the Sr. **c** Unoccupied p_z state on the original surface dimer. **d** One of many unoccupied Sr *d*-character states. Reprinted figure with permission from Ref. [17]. Copyright (2009) by the American Physical Society (Color figure online)

Equally promising is the fact that Si can be grown epitaxially on a $LaAlO_3$ substrate, although the fact that the growth mode is three dimensional (instead of two-dimensional) suggests the interface is unstable (see Fig. 9) [41, 42]. Finally, $LaAlO_3$ can be grown indirectly on Si by first growing a buffer layer of SrO or $SrTiO_3$ on Si [43–46]. Unfortunately, at present there is no experimentally verified method for depositing $LaAlO_3$ epitaxially and directly on Si.

In the authors' view, there are two main obstacles to the growth of $LaAlO_3$ directly on Si. First, in the same way that Sr is used to passivate the Si surface to enable the growth of SrO or BaO or $SrTiO_3$, the Si surface must be passivated in order to prevent undesired reactions between the Si substrate and the La, Al, and O during growth. Second, unlike $SrTiO_3$, $LaAlO_3$ is polar along the (001) direction, so that any stable interface (and surface) must compensate the polar field in some way. In this section, we discuss what happens when La is used instead of Sr to passivate the surface, and address issues related to the polar field in the next Section (Sect. 2.6).

Initial studies used DFT to investigate the binding of submonolayer coverages of La to the stoichiometric dimerized Si (001) surface [47]. Similar to Sr on Si, one finds that (i) La has a low energy binding site in the trough between four Si dimers, (ii) at low coverages La adatoms occupy these binding sites, (iii) the La adatoms form a variety of chain-like structures, and (iv) that the La-on-Si system has a highly stable structure when there is one La valence electron per dangling Si orbital. However, due to its extra valence electron on La compared to Sr, this stable structure occurs at 1/3 ML La coverage instead of 1/2 ML. This 1/3 ML structure has even stronger covalent character than the analogous Sr-on-Si structure, with significant occupation of La *s*, *d*, and *f* states despite the La being formally in the +3 state [20]. This extra covalent interaction results in a binding energy to the Si surface per La which is 88% larger than for Sr despite the fact that La only has 50% more valence electrons than Sr [20].

While the results for La on a stoichiometric Si surface are qualitatively similar to the those for Sr on Si, when the phase space is enlarged to include structures with non-stoichiometric silicon coverages, significant differences emerge [20]. In particular, a series of 2/3 ML La-silicide structures become stabilized. Since La has three valence electrons, these structures would be electron rich on a stoichiometric Si surface and would force the La into an unfavorable +2 state. However, the surfaces are stabilized by adding extra Si atoms to the surface. Each extra Si atom with its two half-filled dangling orbitals accepts the "extra" two electrons from the La, which returns the La to the favorable +3 state, and lowers the total energy. In fact, these structures are so stable that they completely modify the phase diagram and exclude the 1/3 ML La structure from forming. Instead, at coverages near 1/3 ML La, the surface is predicted to phase separate into lower coverage chains and the 2/3 ML silicide structure. The 2/3 ML La structure and the electronic redistribution are illustrated in Fig. 10.

In order to form these non-stoichiometric silicide structures, Si must rearrange on the surface. As discussed above in Sect. 2.3, on a bare silicon surface, the large energy barrier for Si motion would require high temperatures so that Sr is needed to catalyze the Si mobility. However, La is even more effective than Sr at lowering Si

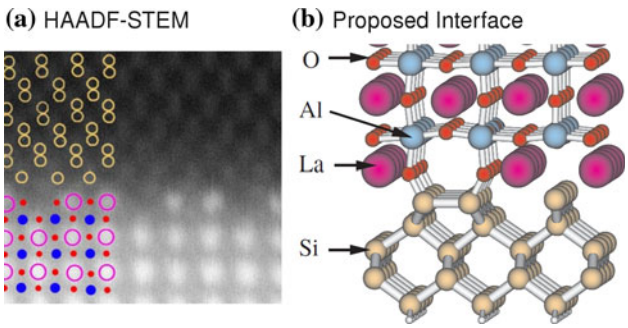

Fig. 9 **a** Experimental interface of Si grown on $LaAlO_3$ with high angle annular dark field imaging (HAADF) scanning transmission electron microscopy (STEM). The interface has a 3 × 1 reconstruction, with 2/3 ML La (*magenta* La, *blue* Al, *red* O). Reprinted figure with permission from Ref. [41]. Copyright (2005) by the Japan Society of Applied Physics. **b** Theoretically proposed interface structure. The two interfacial oxygen will be absent for low oxygen chemical potential growth. Reprinted figure with permission from Ref. [42]. Copyright (2005) by the American Physical Society (Color figure online)

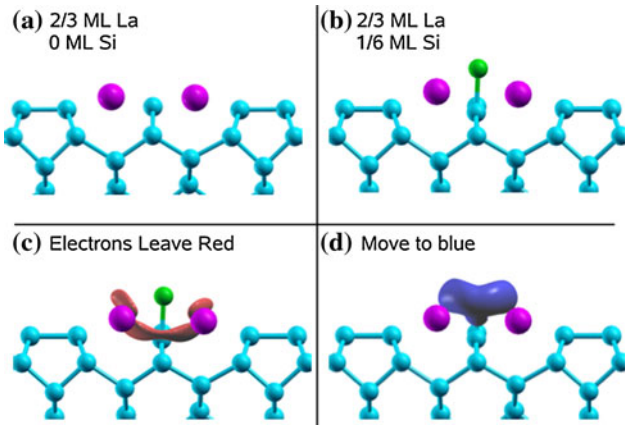

Fig. 10 Side views of two 2/3 ML La-on-Si structures. **a** 2/3 ML La on a stoichiometric Si surface (no Si added) but where the surface has one intact dimer and one broken dimer per unit cell. **b** Highly stable 2/3 ML La broken dimer structure with 1/6 ML Si added (added Si in *green*). **c**, **d** (Smoothed) electron density redistribution plots for structure **b** due to the addition of the Si. When the Si is added and allowed to interact with the surface, electrons leave the *red regions* around the La as shown in **c** and move to the *blue regions* around the added Si as shown in **d**. From Ref. [20] (Color figure online)

kinetic barriers [20]. Increasing La coverage from 0 to 0.5 ML La reduces the energy barrier for Si dimer breaking from 1.29 to 0.37 eV. A barrier of 0.37 eV is low enough to allow significant Si motion even during room temperature deposition. Therefore, it would appear that direct use of La as a passivating metal on Si will likely fail due to the rapid formation of complex (and likely disordered) silicide surface structures that are not ideal for epitaxial growth. And, to date, no experimental growth procedure for epitaxial oxides on Si has been devised with La on Si.

Growth of $LaAlO_3$ on Si

Given the tendency of the La on Si system to form high coverage La-silicide structures discussed above, attempts to grow $LaAlO_3$ on Si that begin with La deposition seem doomed to fail. In this section, various methods that may circumvent this difficulty are discussed. Separately, along the (001) growth direction, $LaAlO_3$ is polar because the LaO and AlO_2 atomic planes that form $LaAlO_3$ have formal charges of $+1$ and -1, respectively. This means that a stoichiometric surface or interface of $LaAlO_3$ will lead to a strong polar field in the oxide film that must be compensated in some way. Hence, to form a stable interface between Si and the $LaAlO_3$ film, care must be taken to compensate this polar charge imbalance. This is most effectively achieved by chemical modification of the interfacial layers (doping or substitution of the interfacial atoms).

One proposal for passivating the surface for $LaAlO_3$ growth is to first deposit an initial ML of Al [48]. The deposition of Al on Si has been studied both experimentally [49–52] and theoretically [53–56]: the surface is known to form a stable ordered structure at room temperature. Unfortunately, Al reacts with Si at higher temperatures. Furthermore, in order to cancel the polar field through $LaAlO_3$, the substitution of Al for Si at the interface is necessary, but an experimental method for achieving this substitution in a controlled fashion is presently unknown [20, 42, 53]. Another possibility, discussed here, is to use Sr to passivate the surface for $LaAlO_3$ growth [20].

The interface between $LaAlO_3$ and Si (see Fig. 9) has been studied both experimentally using Si grown on $LaAlO_3$ substrates [41] and theoretically using DFT [20, 53]. The interface has a 3×1 reconstruction with 2/3 ML La at and no oxygen at the interface [20]. However, a first-principles thermodynamic analysis shows that while this structure is the lowest energy interface under the constraint of having a two-dimensional interface between the two materials, the interface actually is not thermodynamically stable in that one can always lower the total energy of the entire system by decomposing it into a bare Si surface and the bulk $LaAlO_3$ oxide. This result is consistent with the observed three-dimensional growth pattern [20].

The experimentally observed La-terminated interface layer has four half-filled silicon/oxygen bonds per 3×1 area. However, the two La per unit cell provide six electrons, leading to an electron-rich interface and suggesting that the interface can by stabilized by the substitution of Sr for La [20]. A more complete first-principles thermodynamic analysis suggests that this stabilization is in fact possible, but, instead of a simple Sr for La substitution into the 3×1 structure, the system prefers either the Sr-rich 2×1 interface shown in Fig. 11a or the 1×1 La-rich interface shown in Fig. 11a.

In addition to needing a stable interface, the growth of an epitaxial thin film using a layer-by-layer method such as MBE requires that the surface at each step of the growth process be stable as well. In order to achieve this for $LaAlO_3$, the polar surface of $LaAlO_3$ must be compensated by either adding $+0.5$ elementary charges (for the AlO_2 surface) or -0.5 charges (for the LaO surface) per 1×1

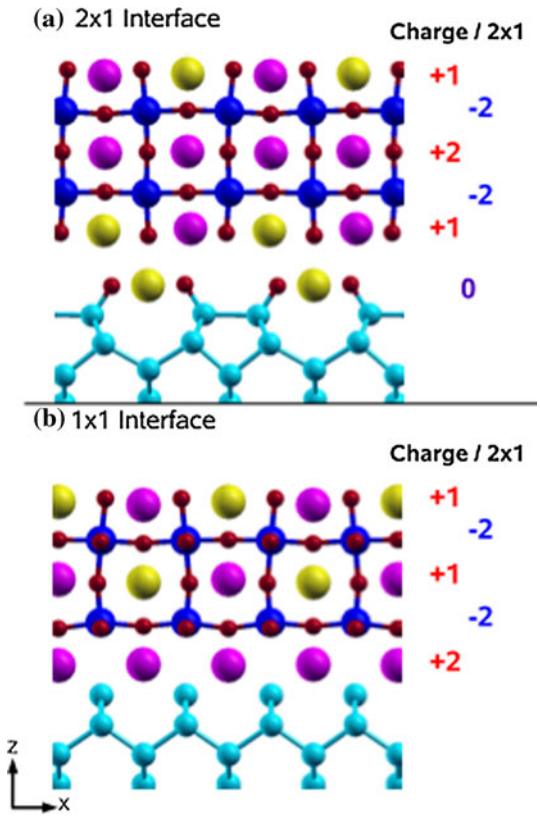

Fig. 11 Side view of two proposed interface and surface structures, as well as the formal ionic charge for each layer per 2×1 area. **a** 2×1 Sr-rich interface. **b** 1×1 La-rich interface. The pattern of formal charges ensures that no long-range polar field exists in the oxide film. Si are *cyan*, oxygen are *small and red*, Al are *medium sized and dark blue*, La are *large and magenta*, and Sr are *large and yellow*. From Ref. [20] (Color figure online)

perovskite surface unit cell. In principle, this can be achieved by incorporating 0.5 ML of Sr into a LaO-terminated surface (see Fig. 11). The 0.5 ML of Sr +2 ions, in concert with the stable interface on the other side of the film, cancels the polar field through $LaAlO_3$, stabilizing the thin $LaAlO_3$ film. Figure 11 illustrates the formal charges for the stabilized interface and surface layers.

The above theoretical considerations suggest the following speculative recipe for growing $LaAlO_3$ epitaxially on Si [20]. To grow the 2 × 1 Sr-rich interface in Fig. 11 a, one would (i) passivate a clean Si surface with 0.5 ML Sr, (ii) lower the temperature and deposit an additional 1.0 ML Sr along with oxygen to form a layer of SrO, (iii) deposit an LaO layer followed by an AlO_2 layer (i.e., 1-unit cell of $LaAlO_3$) and then anneal at moderate temperatures to allow 50% of the La to exchange with the Sr below, and (iv) continue depositing additional unit cells of $LaAlO_3$ at moderate temperatures in order to ensure the the 0.5 ML of Sr "floats" upwards to remain incorporated into the surface layer. This theoretically proposed growth procedure ensures that the interface is stable and that the polar field is at all times compensated. The proposed recipe for growing the 1 × 1 La-rich interface of Fig. 11 b is (i) passivate a clean Si surface with 0.5 ML Sr, (ii) lower the temperature and deposit 0.5 ML Sr, 0.5 ML La at low oxygen pressure to form a disordered layer with Sr, La, and O, (iii) deposit 1-unit cell of $LaAlO_3$ and anneal at modest temperatures to cause 0.5 ML of Sr to "float" to the surface and for the interface to transition from the 2 × 1 Sr-rich phase to the La-rich 1 × 1 phase (similar to the transition seen during the growth of $SrTiO_3$ [6]), and (iv) continue depositing additional unit cells of $LaAlO_3$ at moderate temperatures, again in order to ensure that the 0.5 ML of Sr "floats" upwards to remain incorporated into the surface layer.

While the above speculative recipes are likely to prove challenging to actually realize in an experimental growth procedure, they are presented primarily as a way to show how the entire database of knowledge gained about the kinetics and thermodynamics of Sr-on-Si and La-on-Si can be combined to generate new proposals for growth strategies for epitaxial oxides on semiconductors. In the authors' opinion, the most fruitful way to proceed is to work hand-in-hand with experimental groups to work through the complexities that emerge when any new proposed procedure is tried out in actual practice.

Interfacial properties of epitaxial oxides on semiconductors

Despite the successful experimental growth of epitaxial heterostructures such as $SrTiO_3$/Si [57–61], determining the atomic-scale interfacial structure and predicting how this structure influences the behavior of the oxide thin film remain very difficult in practice. A large number of questions arise: What are the structural, mechanical, and electronic properties of the interface as a system in its own right? How do these properties couple to or modify the thin oxide film and the semiconductor substrate? Do the bulk properties of the oxide still characterize the heterostructure, or does the presence of the interface modify or dominate the oxide's behavior? Over what length scale do the interfacial effects persist? To what extent can the interface properties be controlled by changing the growth procedure and thus the interfacial atomic structure and chemical composition? Can one identify and generalize the chemical and physical principles that govern these behaviors? Various aspects of these questions and our present understanding of their answers are addressed below by a detailed examination of two interfaces: the simpler BaO/Si and the more complex $SrTiO_3$/Si.

In what follows, we will be reviewing the status of the field regarding the above questions and what type of understanding has emerged. First, we look at the challenges of determining the atomic structure of epitaxial complex oxide/semiconductor interfaces in Sect. 3.1. We then briefly review experimental efforts that characterize the heterostructures in Sect. 3.2: the experiments have mainly focused on $SrTiO_3$/Si which represents one of the few complex oxide–semiconductor heterostructures successfully fabricated with an atomically abrupt epitaxial interface. In Sect. 3.3, we review the various $SrTiO_3$/Si interface structures that have been proposed and investigated by first-principles theory. With this background, we then describe the current understanding of the structure and electronic properties of the BaO/Si and $SrTiO_3$/Si systems and the effects of the interfaces on the thin oxide films in Sects. 3.4–3.7.

Challenges in oxide/Si interfacial structure determination

Advances in experimental growth procedures such as MBE and pulsed laser deposition have made it possible to grow coherent epitaxial oxide films with atomically abrupt interfaces on various semiconductor substrates [62]. However, even with knowledge of the atomic layer-by-layer deposition procedure, it is difficult to predict the atomic structure and composition of the as-grown heterostructures. Much of the difficulty stems from the fact that in an oxide/Si heterostructures, the system transistions from a strongly covalent bonding in the silicon to a primarily ionic bonding in the oxide over a length scale of less than a nanometer. A priori, it is unclear what type of interface structure facilitates this transition.

Experimental structural characterization via STEM, RHEED, and XRD provide a great deal of structural information during and after the growth. However, even when used

in tandem, these techniques generally are not sufficient to uniquely determine the atomic-scale structure of the heterointerfaces. One important reason is that the signal intensity from the oxygen anions is much smaller than that from the metal cations, and this leads to difficulty in observing the presence and position of oxygen atoms. In addition, fitting XRD data to solve the atomic structure of a complex interface is a highly challenging endeavor involving a large number of fitting parameters. This is because a great deal of symmetry is broken at an interface and one must fit the positions of atoms in a large number of atomic planes [63].

The use of first-principles computational methods such as DFT *in combination* with experimental characterization allows for a more successful attack on determining the atomic structure of complex heterointerfaces. Once the atomic structure is known with some confidence, DFT can determine the properties of the interface and how they affect the macroscopic behavior of the heterostructure. We note that if one uses theory alone with no experimental input to impose some constraints, it is extremely challenging to predict the structure of complex heterointerfaces as the phase space of possible structures is quite large. For example, Fig. 12 shows only a very small subset of $SrTiO_3$/Si interface structures with small in-plane unit cells—which is the correct one? Furthermore, the structures of interfaces grown via layer-by-layer deposition techniques often correspond to kinetically trapped, out of equilibrium structures which are very hard to identity using standard energy minimization or optimization techniques. In short, understanding the properties of complex oxide–semiconductor interfaces necessitates a great deal of interplay between experiment and theory. The two interfacial examples discussed below show this interplay in some detail.

Previous experimental work

Alkaline earth oxides such as BaO and SrO and the related perovskite oxide $SrTiO_3$ were first grown epitaxially on Si(001) using a layer-by-layer MBE process in 1998 [5]. As described below, $SrTiO_3$ is the most studied epitaxial complex oxide on silicon and one of the few that can be grown as a high quality single crystal. Similar perovskite oxides such as $BaTiO_3$ [64] and $SrHfO_3$ [65] also have been grown on Si(001) but tend to suffer from poor crystallinity. Efforts to grow other epitaxial complex oxide/silicon interfaces, in particular $LaAlO_3$/Si, which is highly desirable because of its larger band gap and favorable band alignments (as per Sect. 2.5), have so far been unsuccessful without an intervening buffer layer between the silicon and the oxide [43–46]. An in-depth experimental review of progress in the growth of complex oxides on silicon can be found in Ref. [6]. It is believed that a detailed understanding of the $SrTiO_3$/Si growth process and the properties of the resulting interface could provide insights for developing new growth processes to enable the growth of more complex oxides on Si and the formation of potentially technologically important heterostructures.

Experiments on $SrTiO_3$/Si

To remind the reader, epitaxial growth of $SrTiO_3$/Si requires the initial deposition of half a ML of Sr atoms [5, 58] which nominally compensate the dangling bonds at the dimerized surface of the silicon substrate [17, 66] and prevent the formation of an amorphous SiO_2 layer at the $SrTiO_3$/Si interface. Additional Sr is then deposited to begin the growth of the $SrTiO_3$ (001) film with a SrO layer. Hence, the initially proposed $SrTiO_3$/Si interface structure [5] as well as a number of other later suggestions [66–68] included an interface buffer layer composed of 1/2 ML of Sr with varying amounts of oxygen sandwiched between the Si substrate and a $SrTiO_3$ film terminated with an SrO layer at the interface. However, TEM and STEM images of the fabricated system indicate the presence of a full ML of Sr at the interface [58, 60, 61] as do the results of XRD experiments [63].

At present, one of the main reasons driving the interest in the $SrTiO_3$/Si heterostructure is the possibility of integrating a ferroelectric $SrTiO_3$ film with a Si substrate to make a FEFET. The potential ferroelectric properties of the heterostructure have therefore received a great deal of attention. Bulk $SrTiO_3$ under the strain that would be imposed by epitaxy on Si was predicted to be ferroelectric near room temperature [69], and experiments have shown that $SrTiO_3$/Si films are definitely polar [61, 70]. Piezo-force microscopy (PFM) measurements on the $SrTiO_3$ surface of the thin films [60] showed indirect evidence that could be interpreted as ferroelectricity. However, direct XRD measurement of the atomic positions in the oxide film [61] demonstrated a temperature-independent and positive polarization (i.e., a polar but non-ferroelectric film). Other PFM studies of the $SrTiO_3$ thin films suggest that defect-driven (relaxor) ferroelectric behavior may be responsible for the observed PFM results [71–73]. Therefore, the immediate questions for first-principles theory are to determine if the $SrTiO_3$/Si system is in fact ferroelectric or not (and if not, why) and more broadly to understand how the oxide-semiconductor interface can control the heterostructure properties. Practically, such knowledge would allow for the development of novel devices that integrate semiconductors with *functional* oxides.

Experiments on BaO/Si

As mentioned above, epitaxial growth of BaO on Si was first achieved in 1998 [5]. As with $SrTiO_3$, in order to grow BaO epitaxially on Si, it is necessary to first deposit a half ML of Sr on the bare Si (001) surface. The atomic structure

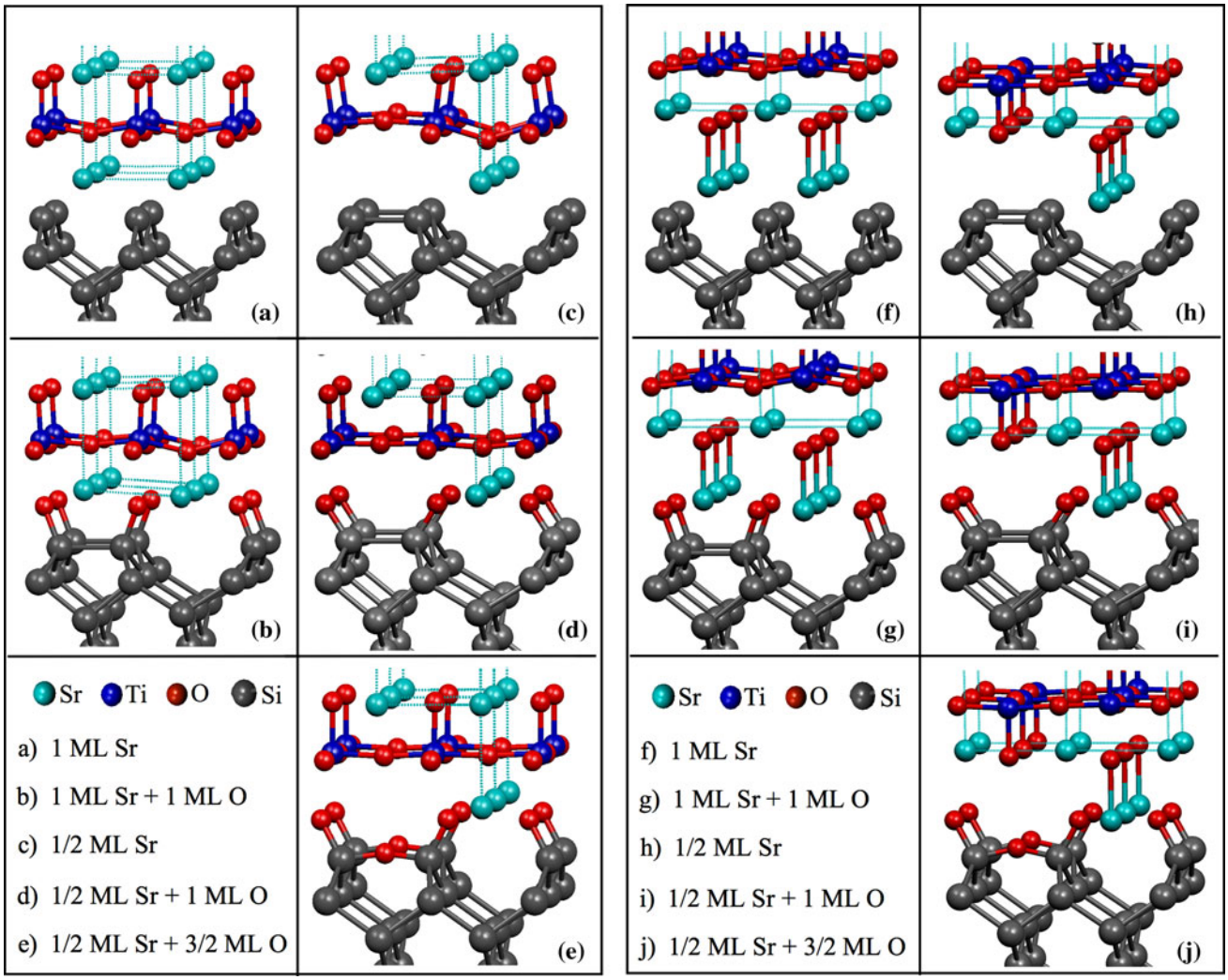

Fig. 12 DFT-computed atomic structures for a number of proposed $SrTiO_3$/Si interface compositions. Si, Sr, Ti, and O atoms are *gray*, *cyan*, *blue*, and *red spheres*, respectively. Reprinted figure with permission from Ref. [75]. Copyright (2011) by the American Physical Society (Color figure online)

of the BaO/Si interface was recently resolved by a combination of XRD and DFT [74]. Due to the ordered nature of the interface (with a 2 × 1 unit cell as observed with RHEED during growth), XRD could directly probe this interface. The experimental difficulty in resolving light atoms such as oxygen and silicon with XRD was overcome by combining the experimental analysis with complementary DFT computations as discussed below.

Previous theoretical work

Theory for $SrTiO_3$/Si

Over the past decade, a variety of structures for the $SrTiO_3$/Si interface have been suggested [57, 66–68, 75–79]. Many of the proposed structures, a number of which are illustrated in Fig. 12, were determined based on charge counting and chemical bonding arguments in combination with DFT calculations. Based on the MBE deposition sequence of the first successful growth procedure [57], many of the initially proposed interfaces [66, 67, 70] had an interface layer with 1/2 ML of Sr atoms passivating the dimerized 2 × 1 Si surface followed by an SrO atomic plane which begins the (001) $SrTiO_3$ film (Fig. 12h). These DFT studies also considered variations with one or more MLs of oxygen inserted into the interfacial Sr layer (Figs. 12i and j). Interfaces consisting of a full ML of Sr with varying amounts of oxygen (Fig. 12b) were also considered [59, 68, 77]. Other works considered the possibility of more complex interfacial kinetics during the growth process and examined structures in which the oxide layer adjacent to the interface is composed of TiO_2 instead of SrO (Fig. 12b [68, 77] and 12d [68]).

A systematic study of 56 distinct interface compositions within a phase space constrained by experimental

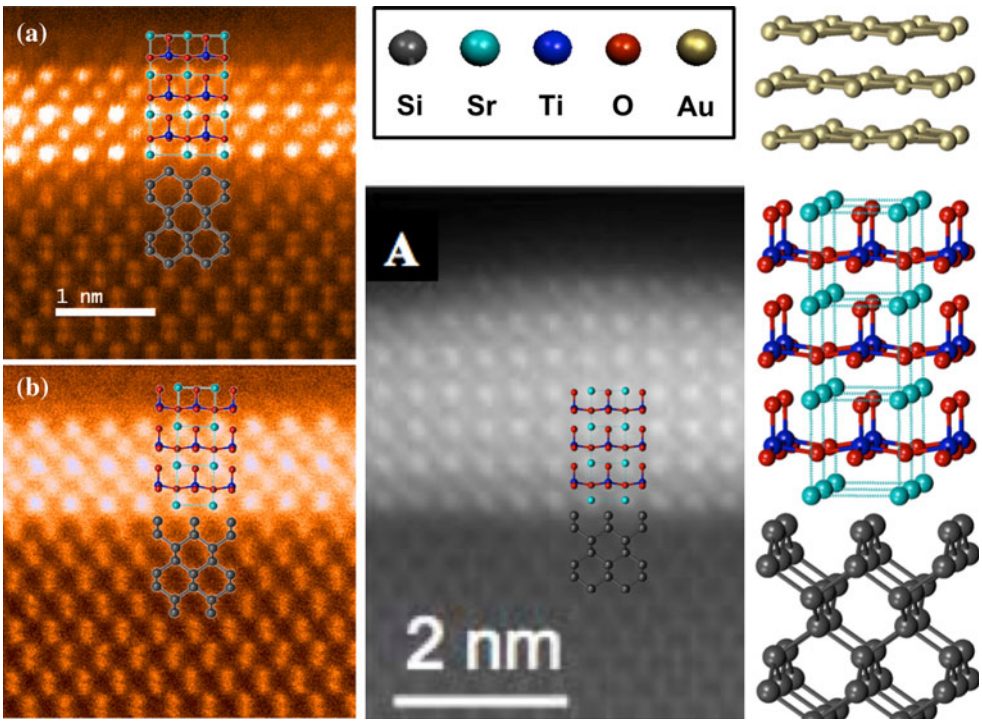

Fig. 13 Structure of the $SrTiO_3$/Si interface. *Left upper and lower panels* comparison of the predicted DFT structure (overlay) with experimental STEM images along the [100] and [010] directions from Ref. [61]. *Center panel* comparison of the predicted DFT structure of Ref. [61] (overlay) with the STEM image along the [010] direction of Ref. [60] which is from Ref. [60] and reprinted with permission from AAAS (Color figure online)

observations (1 × 1 or 2 × 1 in-plane unit cells) was recently performed [61, 75, 76]. This set of structures included all the previously published structures mentioned above as well as a number of new ones (e.g., Fig. 12c, d, f, g). The computed results permitted the construction of a thermodynamic phase diagram for the $SrTiO_3$/Si interface, that in combination with kinetic modeling based on the experimental growth procedures predicted the experimentally-realized interfacial structure (see below for details). The predicted structure (Fig. 12a) matches well with experimental STEM [60, 61] and XRD [61, 63] measurements. It is the only structure in the structural data set that exhibits the four main characteristics identified from STEM images: 1 × 1 in-plane symmetry; lack of Si dimers; 1 ML of Sr at the interface; and a TiO_2 oxide plane adjacent to the interface (Fig. 13). Furthermore, this predicted structure displays significant cation–oxygen displacements in the oxide, the magnitude and direction of which are in agreement with XRD measurements [61] and consistent with the experimental identification of a polar ground state [70].

Theory for BaO/Si

The theoretical structure of the BaO/Si interface was determined using a combination of synchrotron XRD and DFT calculations [74] as mentioned above. The atomic structures of a range of BaO/Si interface compositions consistent with experimental evidence of a 2 × 1 interfacial unit cell and half a ML of Sr atoms at the interface were computed using DFT. Several of the computed structures are illustrated in Fig. 14. It was found that only the structure with half a ML of Sr and a full ML of oxygen at the interface (Fig. 14b) was able to reproduce the main measured XRD peaks, thereby enabling an atomic-scale solution of the interface structure despite the inability of XRD to resolve oxygen atoms. In a later work, comparison of the free energy of the various interfaces coupled with knowledge of the kinetics of oxygen diffusion in the BaO film confirmed that the structure with oxygen at the interface was the one most likely to form during the growth [75]. However, this determination, based on studying a very small portion of the possible structural phase space, would have been completely insufficient to determine the interfacial atomic structure without the complementary and constraining experimental data (and vice versa).

Epitaxial oxides on Si: structure and thermodynamics

One can use computational methods such as DFT to determine the thermodynamic phase diagram of a hetero-interface. As long as a large enough set of structures are computed to form a reasonable representation of the available phase space, the phase diagram can be used to predict the most favorable interface structure under given environmental conditions. In the theory, these conditions correspond to a set of independent chemical potentials for each chemical element in the system [80]. Physically, this means each element in the system is in equilibrium with a physical reservoir such a gas phase, a surface phase, or a bulk phase. To have the epitaxial oxide/Si interface and

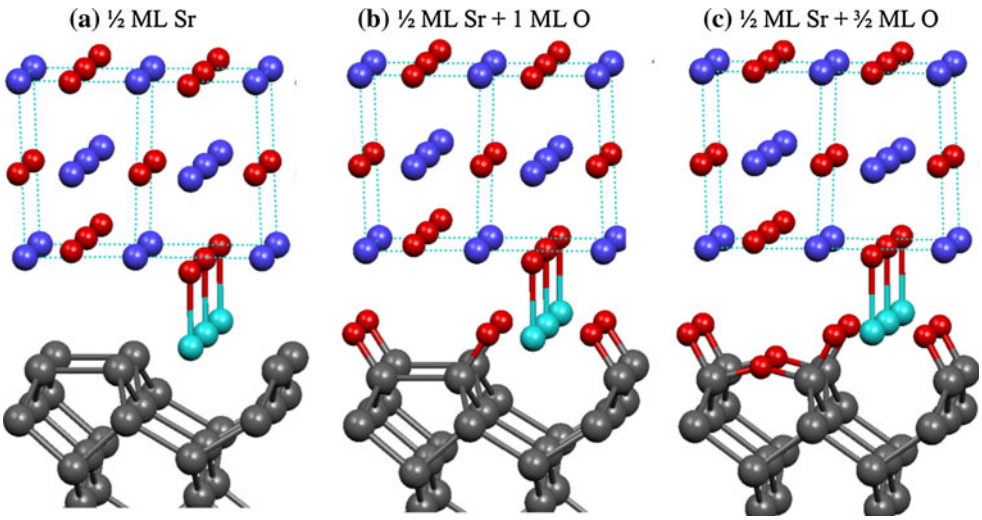

Fig. 14 Computed atomic structures of several BaO/Si interface compositions with 2×1 in-plane symmetry. Si, Ba, Sr, and O atoms are *gray*, *blue*, *cyan*, and *red spheres*. The interface composition per 2D surface cell is indicated. The predicted experimental structure with one monolayer of oxygen at the interface is shown in **b**). Adapted figure with permission from Ref. [74]. Copyright (2009) by the American Physical Society (Color figure online)

heterostructure be at thermodynamic equilibrium requires additional external constraints to be enforced—the most significant is that no bulk SiO_2 phase is present (one of the main goals of the experimental growth is to avoid formation of the deleterious and amorphous SiO_2). The reason for the external constraints is the following: the formation of SiO_2 (taking Si from the substrate and oxygen from the oxide) is so energetically favorable that to thermodynamically inhibit SiO_2 formation, the oxygen chemical potential μ_O or equivalently the oxygen gas partial pressure must be unphysically low. For example, at 873 K, the highest temperature encountered during the growth procedure, the oxygen partial pressure must be at or below 10^{-60} atm which is experimentally inaccessible: typical UHV pressures are $\sim 10^{-13}$ atm. Consequently, any heterostructure at true thermodynamic equilibrium will have a region of amorphous SiO_2 at the oxide/Si interface.

What, then, enables the formation of the abrupt epitaxial interfaces, without amorphous SiO_2, that are observed experimentally? Clearly the interface must be kinetically trapped, but what it the microscopic mechanism? To answer this question, it is fruitful to first compute the thermodynamic interfacial phase diagram and to see which interfaces are thermodynamically stable under various conditions.

The $SrTiO_3$/Si phase diagram

The phase diagram of the $SrTiO_3$/Si interface, computed based on DFT [75], is reproduced in Fig. 15. The diagram shows that once oxygen crosses the interface and Si-O bonds can form, the structure is thermodynamically unstable with respect to bulk SiO_2 formation: the heterostructure can lower its free energy by creating SiO_2 with Si from the substrate and oxygen from the reservoir. At constant μ_O, this process will in principle continue until the entire silicon substrate is oxidized to SiO_2; in practice, the extent of the oxidation and the thickness of the interfacial SiO_2 layer is governed by the rate of oxygen diffusion.

The phase diagram can be used to help determine the experimental non-equilibrium interface structure. For example, Fig. 15 shows that all but one of the interface phases present in the diagram belong to the class of structures with a TiO_2 plane adjacent to the interface layer, suggesting that the interaction between the silicon substrate and the TiO_2 plane plays a significantly role in stabilizing the heterostructure. As a result, one may expect the experimental structure to have this feature. Furthermore, the lack of an interfacial SiO_2 layer tells us that the structure is not in equilibrium with oxygen. Intuitively, the inhibition of oxygen diffusion will make the "local" oxygen chemical potential at the interface be much lower than the oxygen chemical potential in the growth chamber. One might then expect the interface to be trapped in a structure that corresponds to the thermodynamically stable one for very low oxygen chemical potentials.

The structure predicted under this assumption (structure A in the phase diagram of Fig. 6) is in good agreement with experimental characterization, as discussed above and illustrated in Fig. 13. Section 3.5 demonstrates the validity of this assumption of low local oxygen chemical potential at the interface based on the physical properties and kinetics of the interface.

The BaO/Si phase diagram

Applying the same procedure as for $SrTiO_3$/Si and enforcing the same constraint of no amorphous SiO_2 formation at the interface, the thermodynamic stability of various BaO/Si interface compositions has been computed [75]. The phase diagram is reproduced in Fig. 16 which shows the free energy as a function of oxygen chemical

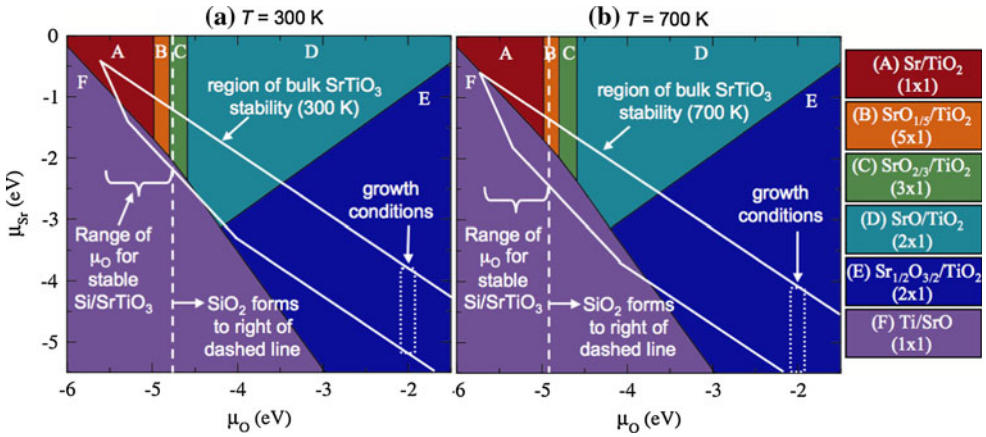

Fig. 15 The DFT-computed $SrTiO_3$/Si interface phase diagram as a function of oxygen and strontium chemical potentials μ_O and μ_{Sr} (the Ti chemical potential is fixed by assuming that bulk $SrTiO_3$ is in equilibrium with the elemental reservoirs). The *white lines* indicate the boundaries of bulk $SrTiO_3$ stability at **a** $T = 300$ K and **b** $T = 700$ K. For each temperature, the vertical white dashed line shows the upper bound on μ_O given by the constraint that no bulk SiO_2 is present in the system. Interface phases to the right of the dashed line are thermodynamically unstable with respect to formation of an interfacial region of bulk-like SiO_2. Reprinted figure with permission from Ref. [75]. Copyright (2011) by the American Physical Society (Color figure online)

potential assuming a fixed amount of Sr (1/2 ML) and that the Ba chemical potential is fixed by having bulk BaO be in equilibrium. As observed for the $SrTiO_3$/Si interface, there is no thermodynamically stable BaO/Si interface without an amorphous SiO_2 region for experimentally achievable μ_O values. As with the $SrTiO_3$/Si system, the experimentally observed abrupt epitaxial BaO/Si interface [74] therefore must correspond to a kinetically trapped structure. The main difference with $SrTiO_3$/Si is that, as shown in Fig. 16, the interface has a much stronger tendency to incorporate oxygen since a "well oxidized" (SrO_2 composition) interface is stabilized before SiO_2 formation is thermodynamically favored. Therefore, one might expect the as-grown BaO/Si interface to have significant oxygen content in the Sr passivating layer.

Epitaxial oxides on Si: kinetics

The $SrTiO_3$/Si interface

Based on an analysis of the growth procedure [75], the initial interface layer is expected to be oxygen poor, i.e., the ratio of oxygen to silicon atoms at the interface should be essentially zero. Therefore, to reach true thermodynamic equilibrium (by attaining a state with an amorphous layer of SiO_2 at the interface), the system must evolve through a structure with oxygen in the interface layer. Namely, for a Si in the interfacial region to be oxidized, an oxygen atom must diffuse from the oxide lattice to the interface (leaving behind an oxygen vacancy) and then from the interface into the Si. Quantitatively, Fig. 17 shows that the energy cost required to form such an oxygen vacancy in the $SrTiO_3$/Si heterostructure is ~ 1 eV lower in the interfacial layer than

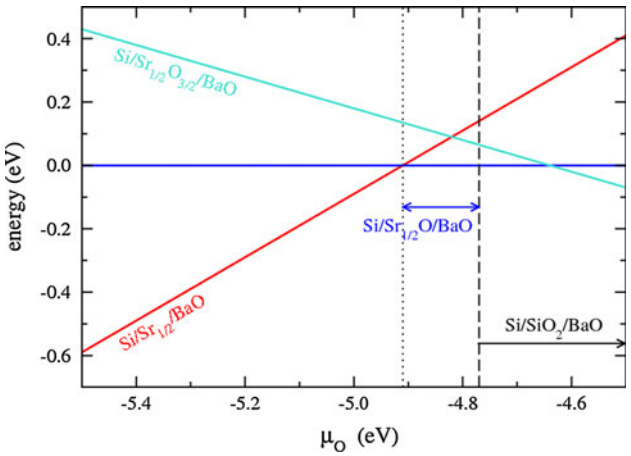

Fig. 16 The BaO/Si phase diagram. The *thin vertical dashed line* is the value of oxygen chemical potential μ_O to the right of which which the interfacial Sr layer begins to incorporate oxygen atoms. The thick vertical dashed line is the μ_O value to the right of which SiO_2 formation becomes thermodynamically favored. The *first line* is to the left of the *second*, meaning the crossover between interfaces with and without oxygen is possible while avoiding formation of SiO_2. Reprinted figure with permission from Ref. [75]. Copyright (2011) by the American Physical Society (Color figure online)

anywhere else in the oxide film. Namely, the oxygen vacancies in the film strongly prefer to be at the interface and there is no local driving force for them to leave the interface which would be necessary to permit oxygen incorporation into the interface. Of course, the overall thermodynamic process whereby an oxygen vacancy diffuses to the surface to be filled by oxygen from the atmosphere does lower the free energy, but clearly the process of vacancy diffusion to the surface is strongly uphill on the energy landscape.

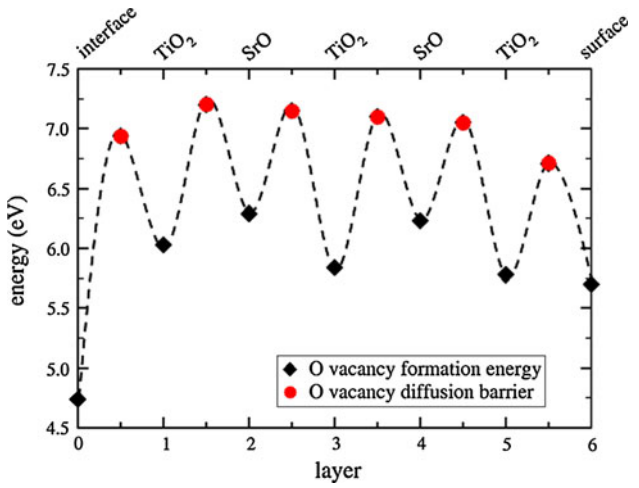

Fig. 17 DFT-computed oxygen vacancy formation energies in each atomic layer (*black diamonds*) and diffusion barriers between adjacent atomic layers (*red circles*) for a 3-unit cell thick $SrTiO_3$ film on Si with 1 ML of Sr and 1 ML O at the interface adjacent to a TiO_2 atomic plane (shown in Figs. 12b, 18b). *Dashed curves* are guides to the eye. Reprinted figure with permission from Ref. [75]. Copyright (2011) by the American Physical Society (Color figure online)

Kinetic modeling based on the DFT vacancy energies and barriers [75] shows that the oxygen poor interfacial structure obtained during the MBE growth is essentially frozen in at room temperature. During the growth which is mostly carried out at 673 K, the system quickly reaches this quasi-equilibrium situation in less than a second where basically all the vacancies migrate to the interface. In this state, the vacancy distribution within the heterostructure is in equilibrium in the canonical distribution (fixed vacancy number), but the vacancy distribution has not reached equilibrium with the oxygen atmosphere. Based on experimentally measured rates of oxygen incorporation on the $SrTiO_3$ surface, the vacancies would be filled by oxygen from the atmosphere only over a much longer time scale of $\sim 10^5$ s ($\sim$30 h) whereas the growth is completed over the time scale of minutes.

The resistance to SiO_2 formation is a direct consequence of the heterostructure interface chemistry. The large position dependence of the oxygen vacancy formation energy arises from the difference in local chemistry between the interface and the interior of the $SrTiO_3$ film [75]. Due to its electronegative nature, oxygen in the heterostructure adopts the 2− anionic valence state, so that removing a neutral oxygen atom from the heterostructure leaves two electrons per vacancy that fill available low energy electronic states. The energies of these available states are dramatically influenced by the local environment (see Fig. 18). When the oxygen vacancy is in the oxide film, the donated electrons fill Ti-derived 3*d* states which form the conduction band edge of the $SrTiO_3$. On the other hand, when the vacancy is located in the interfacial layer, the removal of oxygen creates low energy dangling Si orbitals that are filled by the electrons. The vacancy-donated electrons are much more stable in the latter states which have a lower electronic energy. This underlies the stability of the oxygen vacancies in the interfacial layer.

The BaO/Si interface

As described above, in the BaO/Si system, the phase boundary between the oxidized and unoxidized interface structure is shifted to lower μ_O compared to that in the $SrTiO_3$/Si system (see Fig. 16). This is primarily due to the larger distance between the interface layer and the first BaO layer compared to the distance between the interface layer and the initial TiO_2 oxide layer in the $SrTiO_3$/Si heterostructure. For $SrTiO_3$/Si, an additional bonding

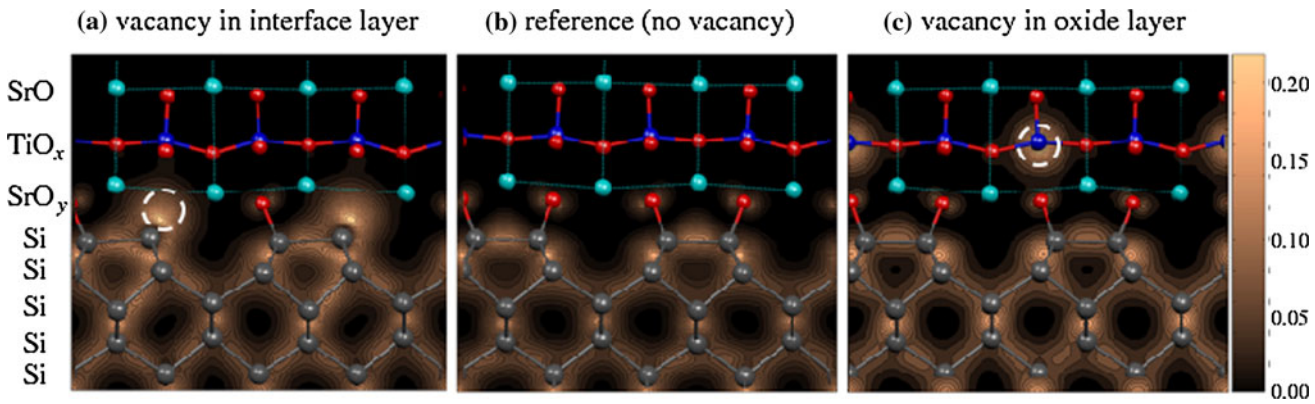

Fig. 18 Integrated local density of states within the SrTiO3 band gap for **a** an oxygen vacancy located at the interfacial layer, **b** the reference structure with no oxygen vacancy, and **c** an oxygen vacancy in the first TiO_2 oxide layer. The vacancy positions in **a** and **c** are indicated by the *dashed lines*. For case **a**, the defect states are dangling Si orbitals as they are highly localized on the Si from which the oxygen is removed. For **c**, the defect states are concentrated in the oxide film and have strong Ti 3d character. Reprinted figure with permission from Ref. [75]. Copyright (2011) by the American Physical Society (Color figure online)

interaction between the Ti 3*d* orbitals and the interfacial Sr/Si states further increases the stability of the oxygen poor state [76]. Consequently, the stabilization of vacancies in the interfacial layer is not as strong for BaO/Si, and oxygen can diffuse more easily to the BaO/Si interface. However, the mechanism by which further oxygen diffusion into the Si substrate is prevented for BaO/Si is unknown. Understanding this difference and what it teaches us about the growth conditions may in turn suggest methods for growing the analogous $SrTiO_3$/Si interface structure. This is very desirable, as oxygen incorporation at the $SrTiO_3$/Si interface changes the electronic energy band alignments across this interface in a direction significantly more favorable for device applications [76].

Interfacial properties

$SrTiO_3$/Si interfacial properties

Previous theoretical work has clearly demonstrated that properties such as the electronic energy band alignment across the interface and the presence or absence of interfacial electronic states, both of which are critical for device applications, are extremely sensitive to the interface structure. For example, a review of DFT electronic structure calculations of $SrTiO_3$/Si [57, 66–68, 76–79] shows that different interface structures result in conduction band energy offsets ranging from -0.2 to $+1.2$ eV and can lead to either insulating or metallic interfaces. Knowing the band offset is helpful but not definitive for determining the interface structure: experimental measurements of the band offset point to a value close to zero for the epitaxial $SrTiO_3$/Si interface [81–83] and allow one to consider eliminating some subsets of the theoretically proposed interfaces.

An investigation of many different $SrTiO_3$/Si interfaces reveals that the large range of band offsets is correlated to the density of bonds between cations in the interface layer and oxygen in the initial oxide layer [76]. For example, the interfacial dipole is decreased and leads to a smaller valence band offset and a larger conduction band offset by either removing interfacial cations (which lowers the lower dipole density) or by adding interfacial oxygens (which screen the dipole) [67]. Conversely, adding interfacial cations or removing interfacial oxygens increases the magnitude of the interface dipole thereby resulting in a larger valence band offset and a smaller conduction band offset. The presence or absence of partially filled states in the interface region, as well as the character and spatial extent of such states, is governed by the details of the interface composition [76].

However, there exist a number of intrinsic "universal" features that persist across all compositions [61, 76]. The features that most significantly impact the electronic properties of the heterostructure are (i) an electronic interface dipole (i.e., electronic charge transfer) that forms between the Si/Sr interface layer and the oxygen in the first atomic layer of the oxide with the positive end of the dipole located in the Si/Sr, and (ii) a relatively large net positive polarization (i.e., cation–anion displacement) in the first oxide unit cell where the positive direction corresponds to the cations shifting away from the Si substrate. Both properties are found to be a direct consequence of the abrupt transition in the bonding properties across the interface: the oxygen in the first oxide layer at the interface is undercoordinated with respect to bulk. As oxygen is highly electronegative, electrons from the interfacial Si/Sr are transferred to the oxygen, leaving the silicon at the interface partially unpassivated. This behavior can be observed in the electron density difference plots shown for a variety interface compositions and structures reproduced in Fig. 19.

The formation of the interface dipole is responsible for inducing the large cation–oxygen displacements observed for all interface compositions in the oxide layer adjacent to the interface: the cations shift away from the positive charge at the substrate Si/Sr surface [61, 76]. DFT calculations where $SrTiO_3$ is replaced by $BaTiO_3$ or $PbTiO_3$ exhibit the same behavior, suggesting that the above physical principles can be extended to many atomically sharp interfaces between silicon and transition metal oxides [61, 76].

BaO/Si interfacial properties

Overall, the interfacial effects in BaO/Si have the same origin and consequences at those for $SrTiO_3$/Si. DFT calculations show that a significant amount of negative charge is localized above the silicon dimers at the interface [6, 74]. This charge repels the oxygen anions that sit directly above the dimers in the first BaO layer, making half of the oxygens shift out of the plane in the direction away from the silicon substrate. In contrast, strong ionic bonds between the other half of the oxygen anions with the interfacial Sr atoms cause the former to shift toward the Si, producing the distinctive BaO rumpling pattern seen in Fig. 14b. Similar interfacial charge rearrangements and the accompanying cation-oxygen rumpling—which propagate several atomic layers into the BaO film in both theory and experiment—are also found for the other computed BaO interface structures (e.g., see Fig. 14a, c).

The band offsets at the various BaO/Si interfaces depend sensitively on the interface composition [74]. Insertion of oxygen into the interface causes the valence band edge of the oxide to shift up in energy by 0.7 eV compared to the interface structure without oxygen. The shift is due to an additional dipole formed between the top layer of silicon and the added interfacial oxygen. Again, this trend is in

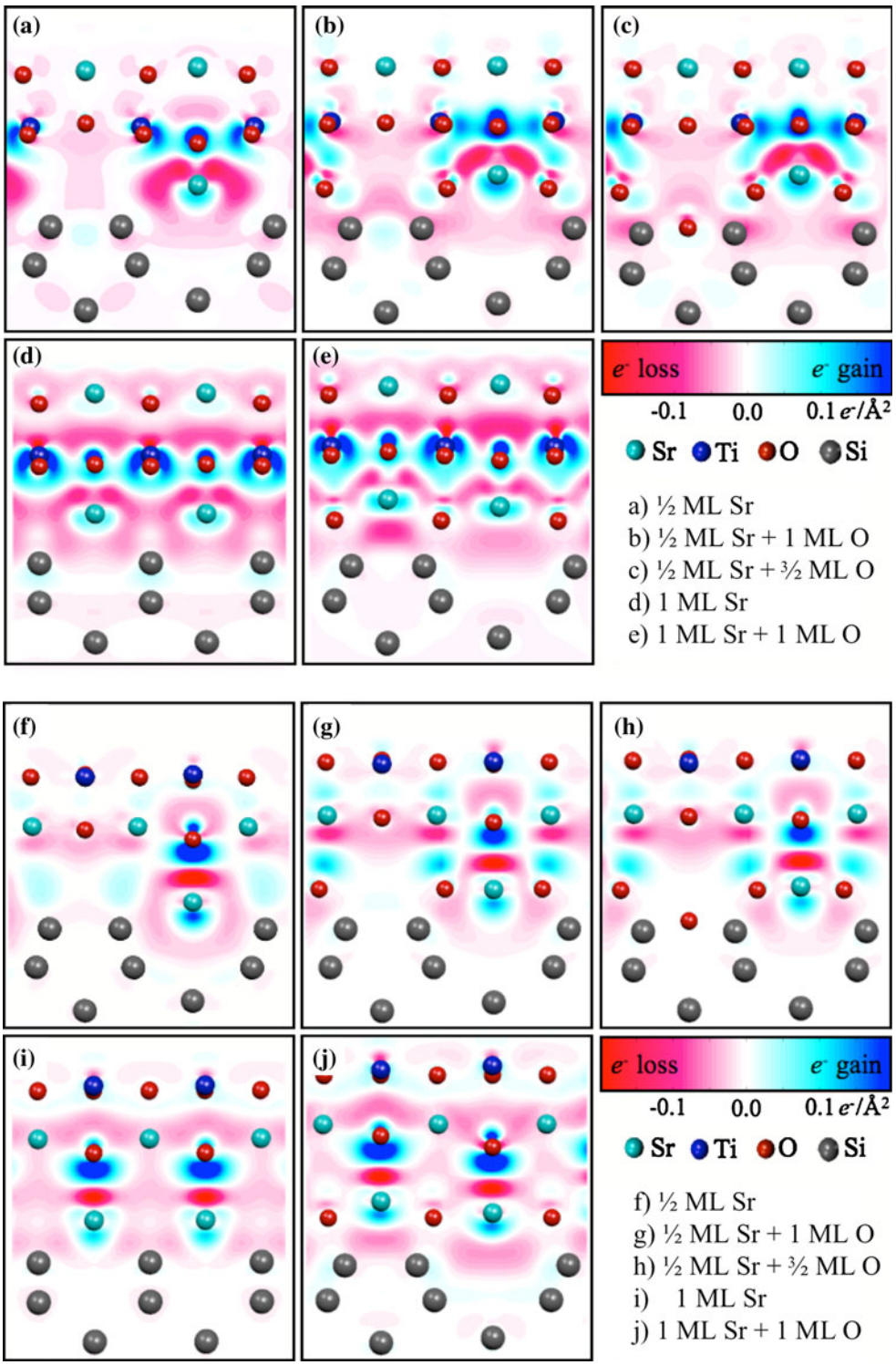

Fig. 19 Electron rearrangement in the *xz*-plane due to interface formation for various $SrTiO_3$/Si (001) interface compositions. *Red and blue contours* indicate electron loss and gain, respectively. In all cases, electrons transfer from the Si/Sr region to the first oxide layer. Atom positions and types are indicated by the superimposed spheres. Reprinted figure with permission from Ref. [76]. Copyright (2012) by the American Physical Society (Color figure online)

agreement with that demonstrated for a range of $SrTiO_3$/Si interface compositions, further demonstrating the fundamental origin and consequent universality of the chemistry governing this type of behavior at oxide-semiconductor interfaces.

Effect of the interface on the oxide film

The universal interfacial features described above—i.e., formation of electronic dipoles and strong polarization of the oxide layers—have important consequences for the

design of FEFETs and other non-volatile devices based on ferroelectricity. First, the formation of the interface dipole creates a bias field across the interface and the associated bias potential must be compensated in some way by the oxide film. Second, the strong interface polarization places additional structural and electrostatic boundary conditions on the heterostructure. Both of these properties markedly favor the positively poled state in the oxide film. Third, and most important, the chemical bonding at the interface is found to pin the polarization in the film in the positive state and render it unswitchable [61, 76].

The interfacial bonding interactions completely dominate the energetics of the $SrTiO_3$/Si system and override any tendency for mono-domain or multi-domain ferroelectricity in the strained $SrTiO_3$ [61]. DFT predicts that the zero temperature ferroelectric well depth for strained bulk $SrTiO_3$ is 23 meV per perovskite primitive cell, which means that at best the $SrTiO_3$ film can gain this much energy per unit cell by forming a ferroelectrically polarized state (mono- or multi-domain). In comparison, when the $SrTiO_3$ is placed on Si and the interfacial bonds are formed, a plot of the energy of the heterostructure versus interfacial polarization shows only a single minimum at positive polarization, and the well depth is 170–600 meV per perovskite 2D surface unit cell compared to the non-polarized state (the variation is over different interface compositions). Furthermore, DFT predicts that multi-domain ferroelectric states, paraelectric states, and negatively poled $SrTiO_3$ states are all *mechanically unstable* and relax directly to the pinned, non-ferroelectric, positively poled ground-state structure.

In essence, the polarization cannot be flipped because the pinned positive interfacial polarization is so robust that no second energy minimum as a function of polarization exists for the system to access. Therefore, these results indicate that this heterointerface—and most likely oxide-semiconductor systems of the same class but with modified ferroelectric oxide or semiconductor materials—cannot be used to couple ferroelectric behavior with the semiconductor substrate.

Another important aspect of the oxide/Si heterostructures is the possible presence of interfacial electronic states. While interface states are not found for every interface composition, they actually are necessary (as charge reservoirs) to stabilize a finite polarization across the entire oxide film: without interface states, the polarization is found to decay quickly to zero away from the interface [76]. This is consistent with previous thin film ferroelectric calculations [84] and phenomenological models [85] that predict a critical thickness below which ferroelectricity is unstable. The requirement of a significant interface density of states (DOS) to stabilize ferroelectricity in this class of heterostructures has enormous implications for the development of various types of transistor devices. On the one hand, without interfacial states the oxide should not be ferroelectric. On the other hand, with interfacial states, even if the oxide has two stable polarization states, the oxide ferroelectric polarization may couple poorly to the doped carriers in the semiconductor substrate because any electrical fields from the oxide polarization will be screened by charge accumulation in the high density of interfacial states. This suggests that a completely new paradigm of interface design might be necessary to develop functioning ferroelectric field effect devices: to create a ferroelectric film on Si, it will be necessary to (i) engineer the structure and composition of interface itself to make it ferroelectric and (ii) consider the role of the interfacial states in device functionality (e.g., the carrier density in the interface layer could be the one modulated by the ferroelectric polarization).

Outlook

The primary task of this review has been to describe the current state of our understanding, based on first-principles modeling, of the growth and resulting properties of epitaxial heterostructures of metal oxides and semiconductors. The two broad topics described were (i) understanding how the initial semiconducting surface must be passivated and prepared to enable the epitaxial oxide to grow, and (ii) describing the physical and chemical properties of the interface and how the interface influences the oxide film. Throughout the review, we have emphasized multiple times how the *simultaneous* application of theory in conjunction with multiple experimental approaches such as MBE growth, diffraction measurements, and high resolution microscopy provides the most fruitful method to solving scientific and engineering puzzles in this domain. Continued research in this general area promises to lead to new physics and phenomena as well as new technologies enabled by integration of the functional degrees of freedom in metal oxides with the well-oiled machinery of semiconductor technologies. The authors see future ab initio work in this field as clustering into three main categories.

First, theoretical research should address the experimental difficulty of growing a large variety of complex oxide thin films epitaxially on semiconductors with atomically abrupt interfaces. This will require the development of a detailed understanding of the kinetic processes during growth as well as an accurate picture of the chemical and physical properties of the interface during each stage of growth. Hopefully the resulting knowledge will enable the fabrication of various desirable heterointerfaces, as exemplified by the case of $LaAlO_3$/Si in Sects. 2.5 and 2.6.

Second, taken to the next level, iterative collaboration between computation and experiment could enable the

development of growth procedures that kinetically trap specific interface structures and chemical compositions. One example of a practical application of being able to design the interfacial structure is to control the technologically important property of electron energy band alignment across the interface. An example of a possible kinetic trapping involves the origin and mechanism of the SrO/TiO_2 switch that happens during the growth of $SrTiO_3$ on Si [75]: this refers to the fact that although the first steps of the growth create SrO layers of the oxide on the Si substrate, once Ti is deposited on top, the system somehow lowers its total energy by having the TiO_2 migrate to the interface and become the first oxide layer. Can one trap the structure to have an SrO interface? Aside from the unsolved mystery of how this rapid and coherent re-ordering occurs, another puzzle is that the switch is apparently *necessary* for epitaxial growth: when the order of the growth procedure is reversed to deposit layers as observed in the final structure, one fails to produce a SiO_2-free interface. In short, understanding and controlling kinetics during growth might allow a much wider set of interfaces to be realized in experiments.

Third, theory and computation will play an important role, again in conjunction with experiment, in the design and growth of novel interfaces that can induce functionality in complex oxide/semiconductor heterostructures. The functionality we focused on in Sects. 3.2.1 and 3.7 was ferroelectricity and the coupling between ferroelectric polarization and semiconductor carrier density which enables a FEFET. Section 3.7 explained how the interface can hinder the desired functionality in the film. The main question is thus if one can overcome the hindrances to enable functionality and if so precisely how to do it. One idea is to use kinetics to modify the interfacial composition and structure of known oxide/semiconductor interfaces to enable functionality. Another interesting direction involves direct chemical modification of the interfacial layer(s) via, for example, cation and/or anion substitution [76]. The main idea of the latter approach is to engineer the interface to have the desired functionality which will then propagate into the oxide and/or couple to the oxide degrees of freedom. The coupling of multiple functionalities (of the interface, oxide film, or semiconductor) could lead to multiple axes of tunability for the heterointerface and thus exploitable multi-functional material behavior.

Acknowledgements We are grateful for extensive collaborative opportunities and numerous discussions with our colleagues including Charles Ahn, Eric Altman, Christine Broadbridge, Victor Henrich, Jason Hoffman, Jay Kerwin, Agham Posadas, James Reiner, Yaron Segal, John Tully, and Frederick Walker. This work was primarily supported by the NSF MRSEC program under Grant No. MRSEC DMR-1119826. Computational facilities were provided by the Yale University Faculty of Arts and Sciences High Performance Computing Center, by the National Science Foundation under Grant #CNS 08-21132 that partially funded acquisition of the facilities, as well as the NSF TeraGrid computer systems.

References

1. Turley J (2002) The two percent solution. Electronic Engineering Times, Dec 18 2002. http://www.eetimes.com/discussion/other/4024488/The-Two-Percent-Solution
2. Wilk GD, Wallace RM, Anthony JM (2001) J Appl Phys 89(10):5243
3. Moore G (1965) Electron Mag 38:4
4. Schaller RR (1997) IEEE Spectr 34:52
5. McKee RA, Walker FJ, Chisholm MF (1998) Phys Rev Lett 81(14):3014
6. Reiner JW, Kolpak AM, Segal Y, Garrity KF, Ismail-Beigi S, Ahn CH, Walker FJ (2010) Adv Mater 22:2919
7. Kolpak A, Walker F, Reiner J, Segal Y, Su D, Sawicki M, Broadbridge C, Zhang Z, Zhu Y, Ahn C, Ismail-Beigi S (2010) Phys Rev Lett 105(21):217601
8. Wolfram T, Ellialtioglu S (2006) Electronic and optical properties of d-band perovskites. Cambridge University Press, Cambridge
9. Looney DH (1957) U.S. Patent 2,791,758
10. Brown WL (1957) U.S. Patent 2,791,759
11. Morton JA (1957) U.S. Patent 2,791,761
12. Ross IM (1957) U.S. Patent 2,791,760
13. McKee RA, Walker FJ, Nardelli MB, Shelton WA, Stocks GM (2003) Science 300(5626):1726
14. Lettieri J, Haeni JH, Schlom DG (2002) J Vac Sci Technol A 20(4):1332
15. Reiner JW, Garrity KF, Walker FJ, Ismail-Beigi S, Ahn CH (2008) Phys Rev Lett 101:105503
16. Ashman CR, Först CJ, Schwarz K, Blöchl PE (2004) Phys Rev B 69(7):075309
17. Garrity K, Ismail-Beigi S (2009) Phys Rev B 80:085306
18. Fan WC, Wu NJ, Ignatiev A (1990) Phys Rev B 42(2):1254
19. Kazzi ME, Delhaye G, Merckling C, Bergignat E, Robach Y, Grenet G, Hollinger G (2007) J. Vac. Sci. Tech A 25(6):1505
20. Garrity KF (2011) Yale Doctoral Thesis
21. Schaadt DM, Yu ET, Vaithyanathan V, Schlom DG (2004) J Vac Sci Technol B 22:2030
22. Li H, Hu X, Wei Y, Yu Z, Zhang X, Droopad R, Demkov AA, Edwards J, Moore K, Ooms W, Kulik J, Fejes P (2003) J Appl Phys 93:4521
23. Shutthanandan V, Thevuthasan S, Liang Y, Adams EM, Yu Z, Droopad R (2002) Appl Phys Lett 80:1803
24. Bakhtizin RZ, Kishimoto J, Hashizume T, Sakurai T (1996) J Vac Sci Technol B 14(2):1000
25. Du W, Wang B, Xu L, Hu Z, Cui X, Pan BC, Yang J, Hou JG (2008) J Phys Chem A 129:164707
26. He J, Zhang G, Guo J, Guo Q, Wu K (2011) J Appl Phys 109(8):083522
27. Liang Y, Gan S, Wei Y, Gregory R (2006) Phys Status Solidi B 243:2098
28. Reiner JW, Segal Y, Garrity KF, Hong H, Ismail-Beigi S, Ahn CH, Walker FJ (2009) J Vac Sci Technol B 27(4):2015
29. Garrity KF, Padmore MR, Segal Y, Reiner J, Walker F, Ahn C, Ismail-Beigi S (2010) Surf Sci Rep 604(9-10):857
30. Alerhand OL, Berker AN, Joannopoulos JD, Vanderbilt D, Hamers RJ, Demuth JE (1990) Phys Rev Lett 64:2406
31. Wang J, Hallmark JA, Marshall DS, Ooms WJ, Ordejón P, Junquera J, Sánchez-Portal D, Artacho E, Soler JM (1999) Phys Rev B 60:4968

32. Zhang X, Demkov A (2008) J Appl Phys 103:103710
33. Smith A, Jonsson H (1996) Phys Rev Lett 77:2518
34. Borovsky B, Krueger M, Ganz E (1997) Phys Rev Lett 78:4229
35. Jonsson H, Mills G, Jacobsen KW (1998) In: Berne BJ, Ciccotti G, Coker DF (eds) Classical and quantum dynamics in condensed phase simulations. World Scientific, Singapore, pp 385
36. Henkelman G, Uberuaga BP, Jonsson H (2000) J Phys Chem 113(22):9901
37. Ramstad A, Brocks G, Kelly PJ (1995) Phys Rev B 51:14504
38. Robertson J (2006) Rep Prog Phys 69(2):327
39. Edge L, Schlom D, Chambers S, Cicerrella E, Freeouf J, Hollander B, Schubert J (2004) Appl Phys Lett 84(5):726
40. International Technology Roadmap for Semiconductors (2007) http://www.itrs.net
41. Klenov DO, Schlom DG, Li H, Stemmer S (2005) Jpn J Appl Phys 44(20):L617
42. Först CJ, Schwarz K, Blöchl PE (2005) Phys Rev Lett 95(13): 137602
43. Xiang W, Lu H, Chen Z, Lu X, He M, Tian H, Zhou Y, Li C, Ma X (2004) J Cryst Growth 271(1–2):165
44. Reiner JW, Posadas A, Wang M, Sidorov M, Krivokapic Z, Walker FJ, Ma TP, Ahn CH (2009) J Appl Phys 105(12):124501
45. Merckling C, Delhaye G, El-Kazzi M, Gaillard S, Rozier Y, Rapenne L, Chenevier B, Marty O, Saint-Girons G, Gendry M, Robach Y, Hollinger G (2007) Microelectronics reliability 47(4–5):540. 14th Workshop on Dielectrics in Microelectronics (WoDiM 2006)
46. Mi YY, Yu Z, Wang SJ, Lim PC, Foo YL, Huan ACH, Ong CK (2007) Appl Phys Lett 90(18):181925
47. Ashman CR, Först CJ, Schwarz K, Blöchl PE (2004) Phys Rev B 70:155330
48. Devos I, Boulenc P (2007) Appl Phys Lett 90:072906
49. Zhu C, Misawa S, Tsukahara S, Kawazu A, Pang S (1999) Appl Phys A 68:145
50. Zhu C, Misawa S, Tsukahara S (1996) J Appl Phys 80:4205
51. Seo J, Park J, Jung S, Yoo KH, Whang C, Kim S, Choi D, Chae K (2006) Chem Phys Lett 417:72
52. Zhu C, Kawazu A, Misawa S, Tsukahara S (1999) Phys Rev B 59:9760
53. Knizhnik AA, Iskandarova IM, Bagaturyants AA, Potapkin BV, Fonseca LRC, Korkin A (2005) Phys Rev B 72:235329
54. Brocks G, Kelly PJ, Car R (1993) Phys Rev Lett 70:2786
55. Umeno Y, Kitamura T (2004) Modell Simul Mater Sci Eng 12:1147
56. Brocks G, Kelly PJ, Car R (1994) J Vac Sci Technol B 12:2705
57. McKee RA, Walker FJ, Nardelli MB, Shelton WA, Stocks GM (2003) Science 300:1726
58. Mi SB, Jia CL, Vaithyanathan V, Houben L, Schubert J, Schlom DG, Urban K (2008) Appl Phys Lett 93:101913
59. Kourkoutis LF, Hellberg CS, Vaithyanathan V, Li H, Parker MK, Andersen KE, Schlom DG, Muller DA (2008) Phys Rev Lett 100:036101
60. Warusawithana MP, Cen C, Sleasman CR, Woicik JC, Li Y, Kourkoutis LF, Klug JA, Li H, Ryan P, Wang LP, Bedzyk M, Muller DA, Chen LQ, Levy J, Schlom DG (2009) Science 324:367
61. Kolpak A, Walker F, Reiner J, Segal Y, Su D, Sawicki M, Broadbridge C, Zhang Z, Zhu Y, Ahn C, Ismail-Beigi S (2010) Phys Rev Lett 105(21):217601
62. Chambers SA (2009) Adv Mater 22:219
63. Kumah DP, Reiner JW, Segal Y, Kolpak AM, Zhang Z, Su D, Zhu Y, Sawicki MS, Broadbridge CC, Ahn CH, Walker FJ (2010) Appl Phys Lett 97(21):251902
64. McKee R, Walker F, Conner J, Specht E, Zelmon D (1991) Appl Phys Lett 59:782
65. Rossel C, Mereu B, Marchiori C, Caimi D, Sousa M, Guiller A, Siegwart H, Germann R, Locquet JP, Fompeyrine J, Webb DJ, Dieker C, Seo JW (2006) Appl Phys Lett 89:053506
66. Forst CJ, Ashman CR, Schwarz K, Blochl PE (2003) Nature 427:53
67. Peacock PW, Robertson J (2003) Appl Phys Lett 83:5497
68. Zhang X, Demkov AA, Li H, Hu X, Wei Y, Kulik J (2003) Phys Rev B 68:125323
69. Haeni JH, Irvin P, Chang W, Uecker R, Reiche P, Li YL, Choudhury S, Tian W, Hawley ME, Craigo B, Tagantsev AK, Pan XQ, Streiffer SK, Chen LQ, Kirchoefer SW, Levy J, Schlom DG (2004) Nature 430:758
70. Woicik JC, Li H, Zschack P, Karapetrova E, Ryan P, Ashman CR, Hellberg CS (2006) Phys Rev B 73:024112
71. Kholkin A, Bdikin I, Ostapchuk T, Petzelt J (2008) Appl Phys Lett 93:222905
72. Leisegang T, Stocker H, Levin AA, Weibach T, Zschornak M, Gutmann E, Rickers K, Gemming S, Meyer DC (2009) Phys Rev Lett 102:087601
73. Yu C, Scullin ML, Huijben M, Ramesh R, Majumdar A (2008) Appl Phys Lett 92:092118
74. Segal Y, Reiner JW, Kolpak AM, Zhang Z, Ismail-Beigi S, Ahn CH, Walker FJ (2009) Phys Rev Lett 102(11):116101
75. Kolpak AM, Ismail-Beigi S (2011) Phys Rev B 83:165318
76. Kolpak AM, Ismail-Beigi S (2012) Phys Rev B (in press)
77. Yakovkin IN, Gutowski M (2004) Phys Rev B 70:165319
78. Demkov AA, Fonseca LRC, Verret E, Tomfohr J, Sankey OF (2005) Phys Rev B 71:195306
79. Robertson J (2006) Rep Prog Phys 69:327
80. Reuter K, Scheffler M (2003) Phys Rev Lett 90:046103
81. Chambers SA, Liang Y, Yu Z, Droopad R, Ramdani J, Eisenbeiser K (2000) Appl Phys Lett 77:1662
82. Amy F, Wan AS, Kahn A, Walker FJ, McKee RA (2004) J Appl Phys 96:1635
83. Chambers SA, Liang Y, Yu Z, Droopad R, Ramdani J (2001) J Vac Sci Technol A 19:934
84. Junquera J, Ghosez P (2003) Nature 422:506
85. Reiner J, Walker F, McKee R, Billman C, Junquera J, Rabe K, Ahn C (2004) Phys Status Solidi B 241:2287